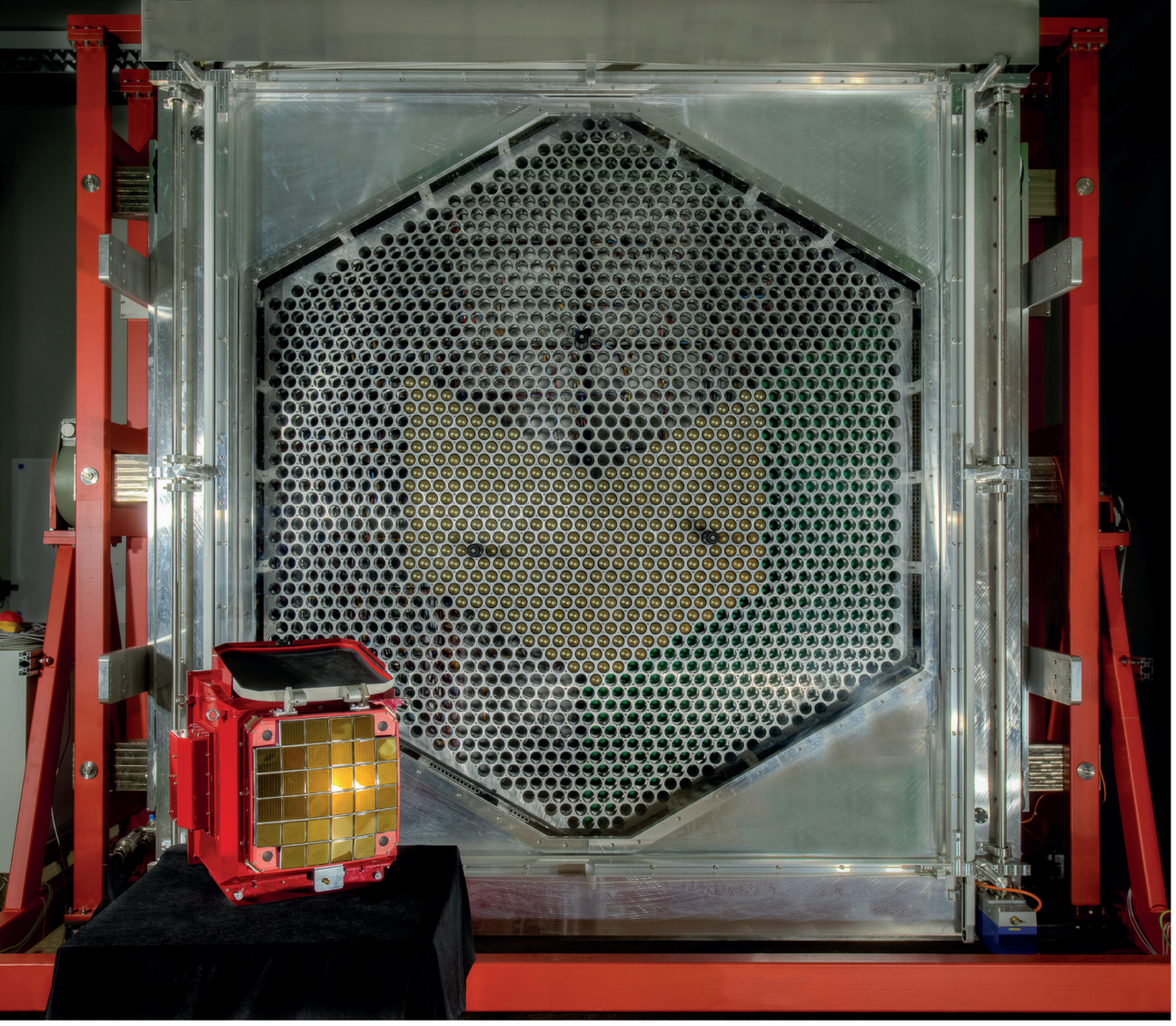

The compact CHEC Cherenkov camera developed for the Small-Size Telescope of the Cherenkov Telescope Array (CTA), in front of the 3 m wide FlashCam camera prototype, for the Medium-Size CTA Telescope.

1.1 Observational Gamma-Ray Astronomy

Introduction

Observational high-energy astrophysics at MPIK is primarily concerned with the study of non-thermal phenomena in the Universe using ground-based instruments to detect very-high-energy (VHE) gamma rays from the cosmos.

Gamma rays in the VHE energy range – with energies in the domain of 10^{12} electron volts – cannot be produced as thermal radiation, like the electromagnetic radiation in most other wavelength regimes; only in the Big Bang were high enough temperatures reached for a very short time. Rather, gamma rays are believed to have their origin in interactions of high-energy cosmic particles with interstellar gas or radiation fields. The high-energy particles themselves – nuclei or electrons – are deflected in Galactic and intergalactic magnetic fields and either cannot reach the Earth at all – in the case of sources in distant galaxies – or will only arrive after a million-year diffusive motion, where they lose all directional information concerning their origin. Imaging the locations where, and identifying the mechanisms by which, particles gain their high energies is hence very difficult. The secondary gamma rays, however, trace the populations of such particles; allowing the cosmic "particle accelerators" to be revealed. Spectral gamma-ray measurements enable the flux and spectrum of the primary particles to be derived.

Owing to the low flux of Teraelectronvolt (TeV, 10^{12} eV) gamma rays – ranging from a few gamma rays per m^2 per year to one per m^2 per century for the sources of interest, detection techniques rely on the Earth's atmosphere to absorb the gamma rays, creating a cascade of secondary particles – an air shower – which are then registered over a large area – some 10^4 to 10^5 m^2 – either directly or indirectly using ground-based detector systems. The development and operation of such detection systems is an essential element of MPIK's programme in astroparticle physics, and is summarised in this section of the report; the scientific results are the subject of the following Chapter 1.2.

Air showers can be detected via the particles penetrating to the ground, via the Cherenkov light and fluorescence light emitted by shower particles in the atmosphere, and via their radio emission. Fluorescence light and radio detection are so far only feasible at ultra-high energies, and have not found application in gamma-ray astronomy. Work at MPIK started – about three decades ago – with ground-based particle detection – the HEGRA and CRT air shower arrays – but then quickly turned to the more promising Cherenkov technique, evolving through three generations of instruments: the HEGRA telescopes, the currently operating High Energy Stereoscopic System H.E.S.S., and the Cherenkov Telescope Array CTA, under construction.

Cherenkov telescopes image the optical Cherenkov light produced by air shower particles, that illuminates a circular area of about 250 m diameter on the ground and can be detected there (Fig. 1). Cherenkov telescopes use large optical reflectors to focus – on dark nights – the Cherenkov light onto a matrix of photon detectors, the "camera". Compared to (at most) m^2-sized satellite-based instruments, which intercept the gamma rays above the atmosphere, Cherenkov telescopes provide huge detection areas of 10^5 m^2 and beyond, governed by the diameter of the Cherenkov light pool; their energy coverage ranges from few tens of GeV to – currently – tens of TeV. At TeV energies, the faintest sources detected have a flux as low as 10^{-13} gamma rays per cm^2 and second. The H.E.S.S. telescope system has been a main contributor to the breakthrough of VHE gamma-ray astronomy in the last

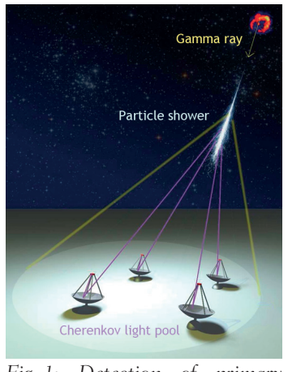

Fig. 1: Detection of primary gamma rays using the Cherenkov light from the gamma-ray induced air showers. The different views of the air shower provided by multiple telescopes allow reconstruction of the shower geometry and hence of the direction of the incident gamma ray.

Fig. 2: The H.E.S.S. telescope system in Namibia, with the four 108 m² telescopes CT1-CT4 operational since late 2003, and the new 614 m² telescope CT5, inaugurated in 2012.

decade; the Cherenkov Telescope Array (CTA) currently under preparation builds upon this success and will provide the next-generation open observatory for gamma-ray astronomy.

Only recently, with the participation in the high-altitude HAWC air shower array, has interest at MPIK in ground-level particle detection systems been revived; instruments such as HAWC cannot match the energy threshold, sensitivity, angular resolution and energy resolution of Cherenkov telescopes, but are complementary in that they provide full-sky coverage, near-100% duty cycle, and allow detection of large-scale emission features that are difficult to disentangle for the limited field of view Cherenkov telescopes.

The High Energy Stereoscopic System (H.E.S.S.)

The H.E.S.S. system of Cherenkov telescopes (Fig. 2) is the primary workhorse of gamma-ray astronomy at MPIK. The system has been operational since late 2003, initially with four telescopes with 108 m² reflector area and 960-pixel cameras, and since 2013 with the additional (H.E.S.S. II) telescope with 614 m² reflector area and a 2048-pixel camera.

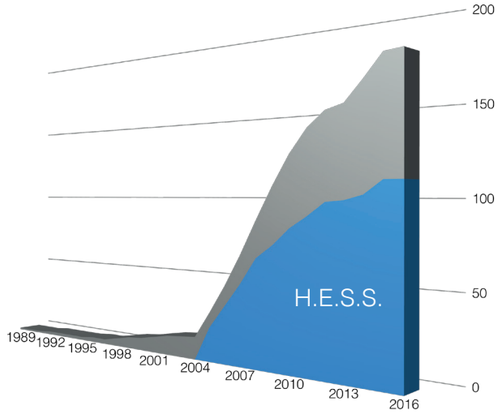

Fig. 3: Discovery of VHE gamma-ray sources over the years; the blue area shows H.E.S.S. discoveries.

In cooperation with other institutes, MPIK provided the structures and drive systems of all telescopes, the mirrors, and the photosensors of the H.E.S.S. I cameras. In late 2016, the electronics of the aging H.E.S.S. I cameras was replaced in an upgrade carried out by DESY, aimed at improving reliability and allowing higher readout rates, relevant if H.E.S.S. I telescopes are triggered in coincidence with the large H.E.S.S. II telescope with its much lower energy threshold – the original H.E.S.S. telescopes provide an energy threshold of approximately 100 GeV, whereas the H.E.S.S. II telescope registers air showers down to 20 GeV gamma-ray energy.

Over the years, the H.E.S.S. telescopes have accumulated 13 700 hours of observations, with a total of 2×10^{10} air showers recorded. MPIK serves as one of the H.E.S.S. data centres; computing capacity and disk space have been continuously upgraded to keep up with the increasing amounts of data and simulations. Figs. 3 and 4 illustrate the discoveries of VHE gamma-ray sources with H.E.S.S., and the sky coverage of H.E.S.S. observations; selected science results are presented in Chapter 1.2.

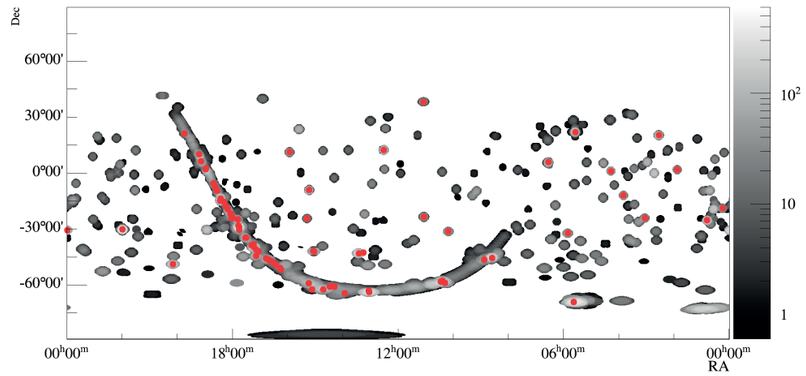

Fig. 4: Sky coverage of H.E.S.S. observations (grey circles, in hours), and H.E.S.S. detections of very-high-energy gamma-ray sources (red points).

The H.E.S.S. II telescope has recorded 2700 hours of data, mostly together with the four H.E.S.S. I telescopes, partly also in stand-alone mode, with the other telescopes observing a different target. Development of data analysis tools proved more time-consuming than expected, due to initial hardware issues, the difficult gamma-hadron separation at low energies, and the challenge of – for the first time – combining data from different-sized telescopes; an exercise that will prove extremely fruitful towards CTA data analysis. Observations in the H.E.S.S. II era focus to a significant extent on steep-spectrum sources such as distant AGN, and on triggered observations of flaring targets such as Gamma-Ray Bursts; the powerful drive system of the H.E.S.S. II telescope and its capability to slew beyond zenith allow typical re-pointing times below one minute. H.E.S.S. II results on a number of science topics are presented in Chapter 1.2.

The Cherenkov Telescope Array (CTA)

The aim of the Cherenkov Telescope Array (CTA) project [1] is the construction of a next-generation observatory for ground-based gamma-ray astronomy (Fig. 5), with a factor 10 better sensitivity than current-generation instruments (Fig. 6). CTA will in addition provide larger energy coverage of over four decades from a few tens of GeV to several 100 TeV, better angular resolution reaching into the few-arcminute regime, and a larger field of view; it will serve as a highly sensitive instrument for surveys as well as for the search for point-like sources and the study of the morphology of extended sources. Full sky coverage will be achieved through the installation of two arrays, one in the southern hemisphere, providing full energy coverage, and a northern array with emphasis on the low-energy instrumentation. To cover the whole energy range in a cost effective way, CTA arrays will consist of over 100 Cherenkov telescopes of different classes with dish diameters of approximately

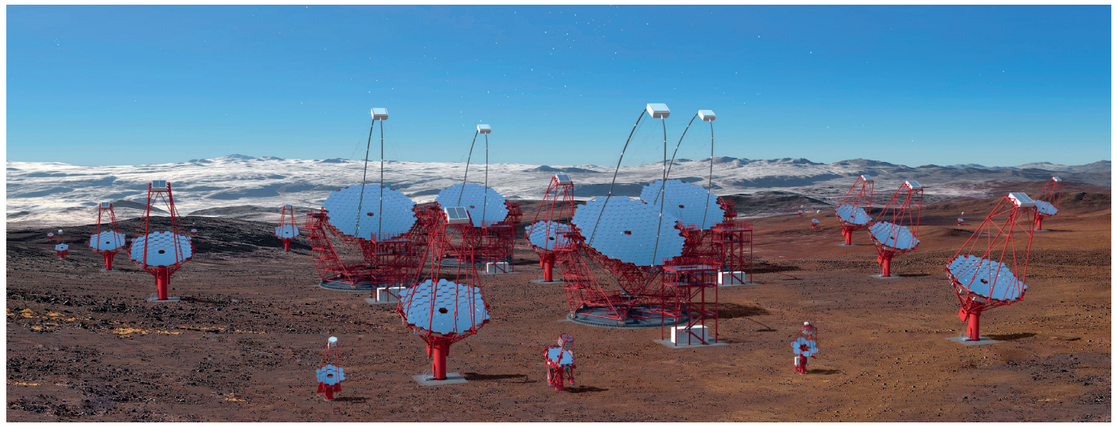

Fig. 5: Rendering of the southern CTA array, combining telescopes of 4, 12 and 23 m size. Credit: G. Pérez, IAC, SMM

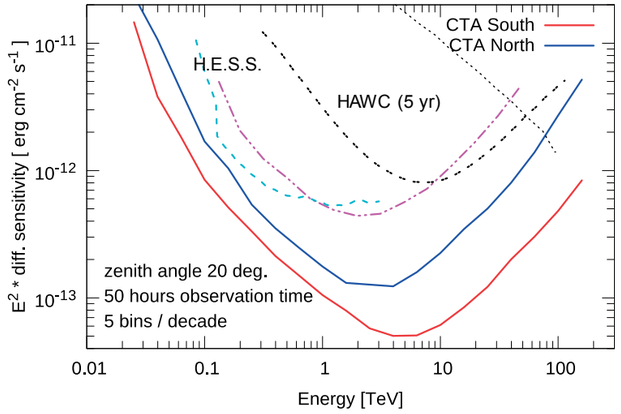

Fig. 6: Energy flux sensitivity of H.E.S.S., of the northern and southern CTA arrays and of HAWC, as a function of energy.

4, 12 and 23 m, distributed over an area of about 5 km² in the southern array and a smaller area in the north. CTA will be the first truly open VHE observatory, providing accessible data products and support services to a wide community.

The Cherenkov Telescope Array (CTA) Consortium formed in 2008, it now (as of late 2016) has grown to over 200 institutes in 32 countries. In 2014, the CTA Observatory (CTAO) gGmbH was founded with its seat in Heidelberg – initially at the Landessternwarte, then at MPIK – as an interim legal entity to prepare for CTA implementation. The CTA project has undergone a series of independent gateway reviews, with the Critical Design Review completed in June 2015. A comprehensive programme of site search and evaluation was conducted from 2010-2013, resulting in a shortlist of sites. In July 2015 contract negotiations began for the hosting of CTA at the European Southern Observatory (ESO) Paranal site in Chile and at the Instituto de Astrofisica de Canarias (IAC), Roque de los Muchachos Observatory in La Palma, Spain. A hosting agreement between CTAO and IAC was signed in September 2016; the agreement with ESO is expected to be signed in early 2017. In June 2016, the CTAO Council selected Bologna (Italy) and Zeuthen (Germany) to host the CTA Headquarters (HQ), and the CTA Science Data Management Centre (SDMC). Signature of an MoU between CTA parties regarding funding of CTA started in October 2016. Infrastructure construction on the sites will start in 2017, in parallel with the deployment of pre-production telescopes aiming to verify mass production, deployment and commissioning, followed by large-scale deployment starting around 2019. Initial user operation of partially-completed arrays is expected for 2021/22.

Major MPIK contributions to CTA concern (i) management: Werner Hofmann has served as Spokesperson since 2008 and was first Managing Director of the CTAO gGmbH (2014-2016), Jim Hinton has served as Project Scientist since 2012; (ii) simulations for the prediction and optimisation of CTA performance; (iii) software development and calibration algorithms; (iv) development and production of the FlashCam Cherenkov camera for the Medium-Size Telescope (MST) and (v) development and production of the CHEC focal plane instrumentation for the Small-Size Telescope (SST).

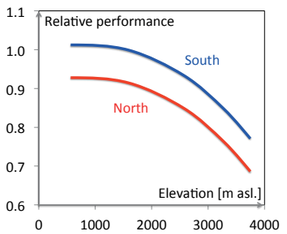

Fig. 7: Relative spectrum-averaged sensitivity of the CTA telescope arrays as a function of site altitude, for northern sites (red) and southern sites (blue), as predicted by detailed simulations. The difference between the northern and southern sites is caused by the larger geomagnetic fields at the northern sites, distorting the development of gamma-ray induced air showers.

Simulating CTA. The design of the CTA arrays is the result of a decade-long, multistep optimisation process, relying heavily on detailed simulations of the instrument, including the development of gamma-ray initiated cascades in the atmosphere, the propagation of Cherenkov light to the telescopes, ray-tracing of the imaging system and the modelling of the electronic signal processing, requiring a massive computational effort [2]. CTA simulations are based on the CORSIKA air shower simulation code interfaced to the *sim_telarray* telescope simulation package developed and continuously improved by K. Bernlöhr at MPIK.

Early studies included semi-analytical estimates and simulations of regular grids; from these studies emerged the need for three telescope sizes to efficiently cover the wide energy range of CTA and address all of the major science questions. The basic characteristics of these telescopes in terms of optical design, photosensor and data capture characteristics were fixed as requirements based on these early simulations, plus a first very-large-scale simulation of realistic CTA telescope arrays. Later large-scale simulations served to assess the site-dependence of performance (in particular site altitude and geomagnetic field) and to establish appropriate telescope spacing. These simulations showed that best performance is obtained by deploying the arrays at altitudes below 2000 m asl (Fig. 7); at lower altitudes, the energy threshold of the arrays increases, resulting in an optimal range around 1500 to 2000 m asl. A final very large simulations effort was used to fine-tune the layouts. In total, MPIK computing systems contributed about 10 million CPU hours to the CTA simulation effort. The final fully optimised telescope arrangement for the southern CTA site is presented in Fig. 8.

Significant effort was furthermore invested in the development of air shower reconstruction algorithms and in the simulation of calibration algorithms. The IMPACT reconstruction algorithm [3], for example, relies on the comparison of measured shower images with a library of image templates. IMPACT provides much improved performance over classical algorithms, as demonstrated with H.E.S.S. data where it is routinely used. Extensive simulations served to demonstrate the calibration of individual CTA telescopes with muon ring images, the cross-calibration of telescopes using air shower events, and the use of cosmic-ray electron spectra for overall array calibration [4].

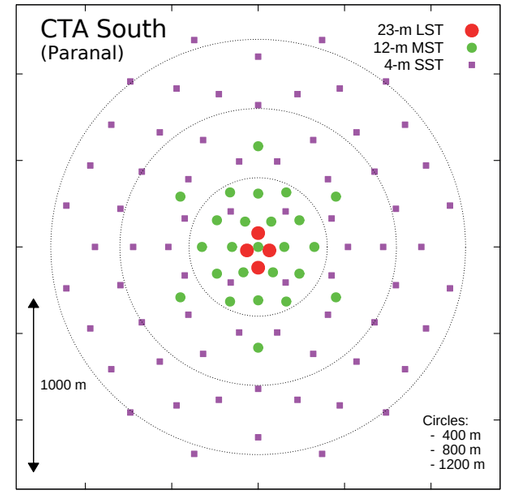

Fig. 8: Baseline layout of telescopes on the southern CTA site, combining 4 Large-Size Telescopes (LST), 25 Medium-Size Telescopes (MST) and 70 Small-Size Telescopes (SST).

FlashCam: a fully digital camera for the CTA telescopes. FlashCam [5] (see title image) is a camera development project for the 12-m medium-size CTA telescope (MST). FlashCam was initiated by the MPIK, and is carried out in cooperation with partner groups from Germany, Switzerland, Austria and Poland. In contrast to "classical" Cherenkov cameras, as installed in current-generation telescopes, the FlashCam concept follows a fully digital approach for the signal processing, using commercially available microchips produced for the growing digital communications market. Besides the mechanical structure, the key building blocks of such a camera are the photon detector plane (PDP), the readout electronics (ROS) and the data acquisition system (DAQ) with the camera server CPU (see Fig. 9).

This functional division provides a high degree of flexibility in the choice of the photosensors or in the detailed layout of the camera. The 1764-pixel photon detector plane (PDP) consists of 147 PDP-modules, each with 12 photomultiplier tubes (PMT). Each module includes high voltage supplies, preamplifiers and a microcontroller for control, monitoring and safety functions. The analogue signals from the pixels are transmitted through standard ethernet cables to the readout electronics. The custom-developed readout electronics of the camera use fast analogue to digital converters (FADC) that digitise the incoming signals continuously with a sampling frequency of 250 MSamples/s and 12-bit resolution. The digitised signals of 24 channels per electronics board are then buffered in a field programmable gate array (FPGA), where the signals are digitally processed and prepared for storage. The key point of this concept is to perform all signal processing based on digitised information. In particular, the trigger decision to store an image is computed in the camera solely from the digitised signals. Depending on the configuration, the total continuous data traffic which is processed within the camera electronics may amount to more than 2 Tb/s. Upon a trigger, the digital image information is then sent to the camera server of the data acquisition system (DAQ), using standard Ethernet components. A water-based cooling system allows the camera to be hermetically sealed, and its temperature to be kept stable.

Together with the project partners, the MPIK has produced a prototype camera (title image and Fig. 10), equipped with the full readout electronics and (so far) about 50% of the photosensors. Based on the experience in assembling and operating the prototype, various details of the design were improved towards mass production. All performance characteristics have been verified in the lab: the prototype meets or exceeds all specifications, including amplitude and time resolution and noise. Deadtime-less readout at up to 30 kHz event rate has been demonstrated. Particular emphasis was placed on verifying the reliability of the design and the long-term stability; the prototype was so far operated in a test environment for well over 1000 hours, including temperature cycling and continuous variation of the orientation of the camera. The next step will be the construction of two pre-production cameras of the final design; for deployment and operation on the CTA southern site. In total, it is planned to build 15 cameras, with MPIK serving as the site for assembly, integration and test.

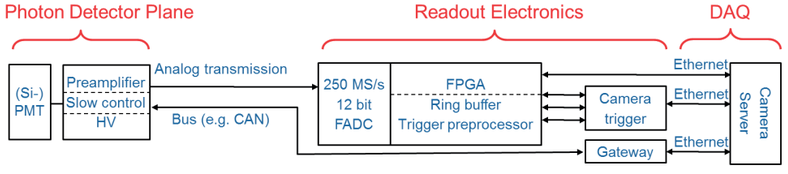

Fig. 9: Basic building blocks of a FlashCam camera.

Fig. 10: Rear view into the FlashCam body, showing in the centre the photon detector plane modules, and in racks left and right the Flash-ADC modules and trigger processors.

Fig. 11: The prototype of the GCT telescopes in Paris-Meudon, during the inauguration on Dec. 1, 2015. Insert: The CHEC Cherenkov camera, see also title image.

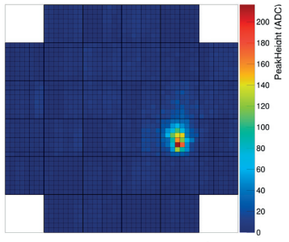

Fig. 12: One of the first Cherenkov images recorded by the CHEC camera on the GCT telescope, during testing in November 2015.

The CHEC camera for the small-size telescopes. The Compact High Energy Camera (CHEC, see title image and Fig. 11) [6] is a development project for the dual-mirror small-size telescopes (SST-2M) of the Cherenkov Telescope Array (CTA), involving MPIK and UK, US, Japanese, Australian and Dutch institutes. The short focal length of the dual-mirror optics of these telescopes results in a very compact camera, with curved focal plane of diameter ~35 cm providing an 8° field of view. The CHEC camera in its first prototype uses multi-anode photomultipliers (MAPMs); a second prototype and the production units will use silicon photomultipliers, with a total of 2048 pixels. For signal capture, the CHEC camera employs the TARGET ASIC, a 16-channel analogue pipeline with a depth of 16 000 samples, operated at 1 GHz sampling frequency. The CHEC camera is built up of 64-channel modules, each module containing the sensors, preamplifier circuits, four sets of TARGET sampling and trigger ASICs, voltage generators for the sensors, digitisers and an FPGA for control and readout. MPIK contributions include software for testing, calibration and operation, extensive testing and characterisation of the prototypes, and optimisation of the mechanical design and of the water-based cooling system of the camera. Together with the other partners, the current plan is to provide 50 CHEC cameras, with MPIK serving as the primary site for assembly, integration and test.

On 26 November 2015, the prototype of the CHEC camera, mounted on a prototype (4-m diameter) SST-2M telescope (Fig. 11) recorded CTA's first ever Cherenkov light while undergoing testing at the Observatoire de Paris in Meudon, France (Fig. 12).

Improving the High Altitude Water Cherenkov (HAWC) Observatory

Compared to past ground-based shower particle detectors, the High Altitude Water Cherenkov (HAWC) gamma-ray detector has achieved a dramatic increase in sensitivity by combining (a) a high-altitude location at 4100 m asl. in Mexico, (b) tightly packed detectors covering about 60% of the 20 000 m² array area, and (c) the calorimetric detection of ground particles using deep water Cherenkov detectors, allowing to – at least partially – identify muons among the shower particles, using those to veto hadron-induced showers. HAWC consists of 300 water Cherenkov detectors of 7.3 m diameter and 4.5 m height (Fig. 13); the tanks are filled with high-purity water and each contain four photomultipliers anchored at the bottom, detecting the Cherenkov light emitted by shower particles in the water. The shower direction is reconstructed using the arrival time of the signals in the different tanks, with a precision ranging from 1° to 0.2° depending on the number of tanks hit; the sensitivity of HAWC is illustrated in Fig. 6 in comparison to H.E.S.S. and CTA.

The performance of HAWC is partly limited by the relatively small size of the detector array, which implies that most showers are detected at the periphery of the array where it is difficult to distinguish between a low-energy shower with its core just inside the array, and a high-energy shower with core position far outside the array, but with a tail of its energy deposition within the array. This has resulted in the plan to add a sparse outrigger array, allowing higher-energy showers outside the array to be identified. MPIK joined HAWC in early 2016, contributing to the outrigger array as well as working towards improved algorithms for data analysis. With six members, the MPIK group is already among the larger HAWC groups. The outrigger array [7] (Fig. 14) consists of 300 smaller water tanks of 1.7 m diameter and 1.6 m height. The outrigger tanks are read out by the MPIK-developed FALCON flash-ADC system, that is based on the modules developed for the FlashCam Cherenkov camera. The ability to record waveforms – rather than time over threshold as for the current HAWC readout – provides a further opportunity to identify penetrating muons and to reject cosmic rays. Significant simulation effort was invested at MPIK towards optimising the geometry and instrumentation of the outrigger tanks.

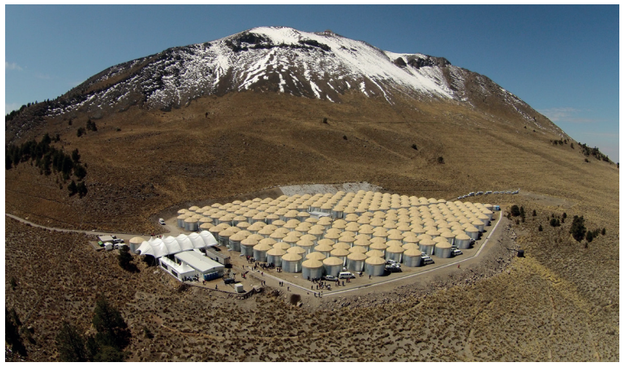

Fig. 13: Overview of the HAWC array of water Cherenkov detectors, located on the Sierra Negra in central Mexico, at 4100 m asl. Credit: HAWC Collaboration

A key motivation for joining HAWC was to gain experience towards the longer-term goal of implementing a wide field of view, large duty cycle detection system in the southern hemisphere, that would complement CTA in several ways, for example providing triggers for CTA observations of variable sources. A water Cherenkov array similar to HAWC, but at even higher altitude (~5000 m asl.), of larger footprint (~50 000-100 000 m²) and with depth-segmented detectors for optimised identification of shower muons would further boost performance, at – in comparison to CTA – relatively modest cost.

Konrad Bernlöhr, German Hermann, Jim Hinton, Werner Hofmann, Michael Panter, Richard White

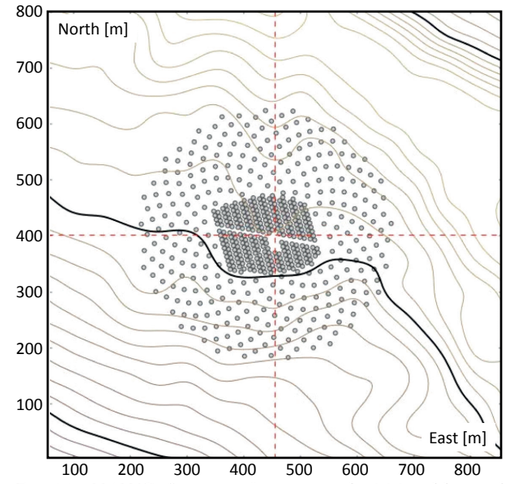

Fig. 14: HAWC "outrigger" array with 300 additional water Cherenkov detectors, currently under construction.

References:

[1] W. Hofmann & CTA Consortium, Proc. XIV Marcel Grossmann Meeting, Rome (2015) and Proc. 6th International Symposium on Gamma-Ray Astronomy, Heidelberg (2016)

[2] G. Maier et al., Proc. 34th International Cosmic Ray Conference (ICRC 2015), The Hague, arXiv:1508.06042 and T. Hassan et al., Proc. ICRC 2015, arXiv:1508.06075

[3] R.D. Parsons and J.A. Hinton, Astroparticle Physics 56, 26-34 (2014)

[4] A. Mitchell et al., Astroparticle Physics 75, 1-7 (2016) and R.D. Parsons et al., Astroparticle Physics 84, 23-28 (2016)

[5] G. Pühlhofer et al., Proc. ICRC 2015, arXiv:1509.02434 and F. Werner et al., Proc. 9th Int. Workshop on Ring Imaging Cherenkov Detectors (RICH 2016), Bled

[6] A.M. Brown et al., Proc. SPIE Astronomical Telescopes and Instrumentation, Edinburgh (2016), arXiv:1608.03420 and J.J. Watson et al., Proc. 6th International Symposium on Gamma-Ray Astronomy, Heidelberg (2016), arXiv:1610.01452

[7] A. Jardin-Blicq, V. Joshi, Proc. 6th International Symposium on Gamma-Ray Astronomy, Heidelberg (2016), arXiv:1610.08340

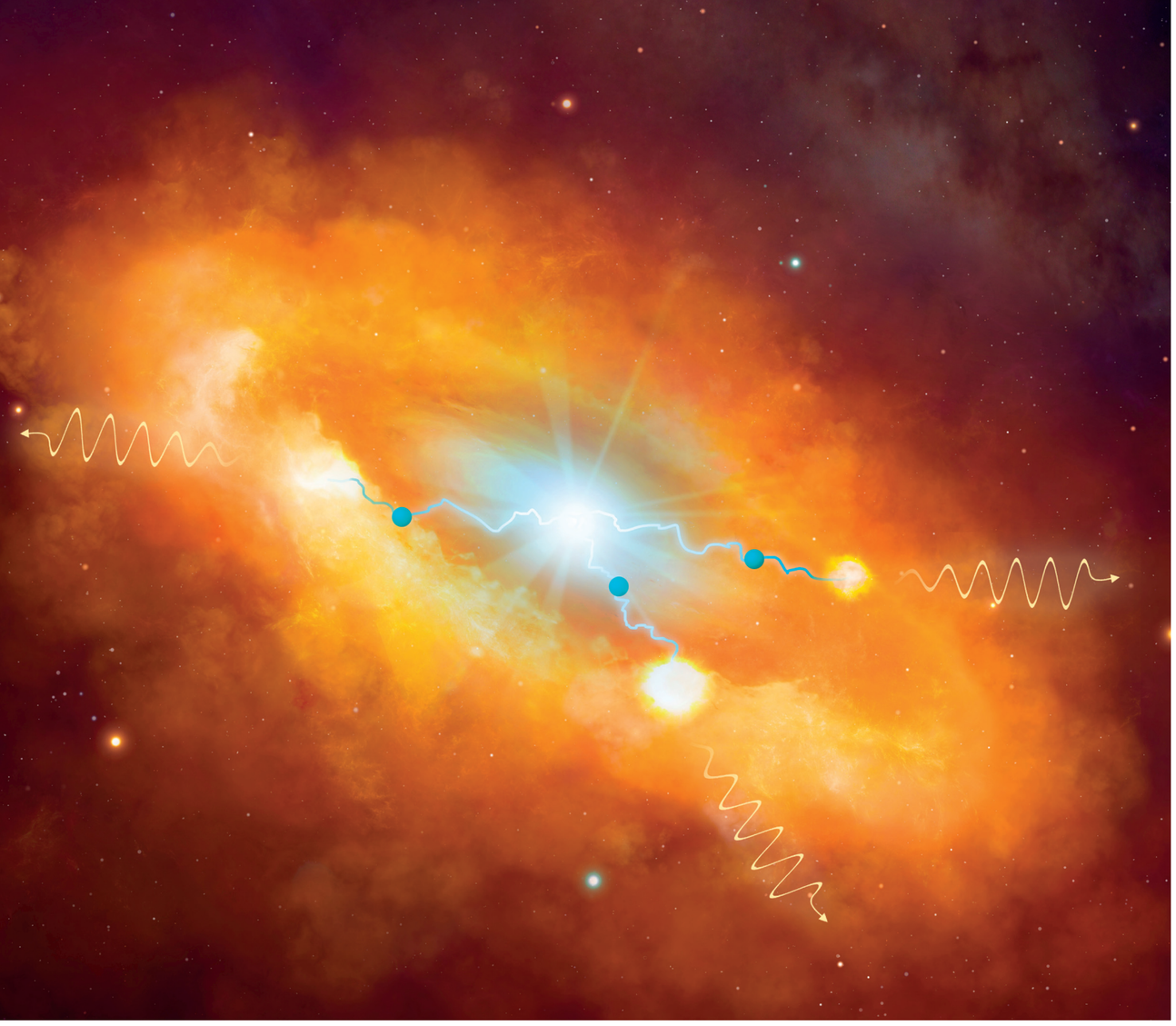

1.2 Non-Thermal Astrophysics

Artist's impression of the giant molecular clouds surrounding the Galactic Centre, bombarded by very-high-energy protons accelerated in the vicinity of the central black hole and subsequently shining in gamma rays. (© Dr Mark A. Garlick/ H.E.S.S. Collaboration)

Introduction

The MPIK conducts a broad observational and theoretical programme in the area of non-thermal astrophysics: the study of relativistic particle populations in the cosmos. Our research covers the acceleration of such particles, their propagation, interactions and radiation processes. The objective is to gain insights into the extreme environments where acceleration takes place, and into the broader role and impact of relativistic particles on astrophysical systems on all scales. The main observational probe employed for such sources is high-energy gamma-ray emission (see Chapter 1.1), but our activities also involve observations at many other wavelengths, probing for example non-thermal synchrotron emission, but also thermal emission that allows us to constrain the properties of cosmic particle accelerators. These observations are complemented by a broad theoretical programme; ranging from fundamental processes to detailed modelling of specific astrophysical objects. Below the programme is summarised by astrophysical target, with theoretical, phenomenological and observational results discussed together.

The Milky Way

The Milky Way clearly represents an excellent opportunity to study the non-thermal astrophysics of star-forming galaxies in great detail. The work at MPIK includes γ-ray surveys and modelling of radiation fields for use in calculating the inverse Compton emission, described in this section, as well as studies targeted at specific object classes or regions.

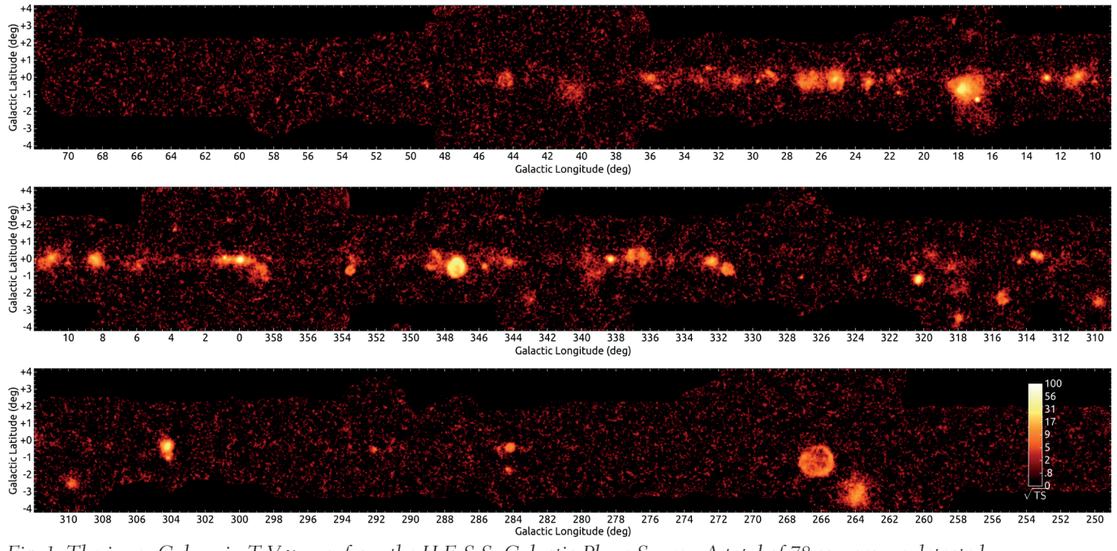

Fig. 1: The inner Galaxy in TeV γ rays, from the H.E.S.S. Galactic Plane Survey. A total of 78 sources are detected.

Gamma-ray source-populations in our Galaxy: The H.E.S.S. Galactic Plane Survey (HGPS) is a major long-standing project within H.E.S.S., led by the MPIK, which is now complete. Data from the first phase of H.E.S.S., collected from 2004 to 2013 provide a total of 2700 hours of high-quality observations of the Galactic plane in the Galactic longitude range of 250° to 65° and Galactic latitude range of $-3.5° < b < 3.5°$. This dataset represents the first high-resolution (0.1°) and sensitive (1.5% Crab nebula point-source sensitivity) survey of the Milky Way in TeV γ rays.

Fig. 1 shows the γ-ray image derived from the HGPS observations, revealing a diverse population of cosmic particle accelerators in the Galaxy. To decompose the emission and create a source catalogue, a robust multi-step procedure was implemented, accounting for the diverse source morphologies and, in certain regions, the high density of sources. A large-scale emission model was constructed, to account for the underlying diffuse emission in the Galactic plane and a multi-scale source likelihood detection and characterisation was performed using an empirical Gaussian assumption for the source morphology. Identified Gaussian components with large overlaps were merged into multi-component sources, and a spectral analysis was performed for each source.

The upcoming HGPS paper (now under internal collaboration review and expected to be submitted early in 2017) presents the analysis and results, and will be accompanied by the release of survey images and a source catalogue in machine-readable format, a first for TeV γ-ray astronomy. The HGPS catalogue contains 78 TeV γ-ray sources, of which 31 are identified as pulsar wind nebulae, supernova remnants or γ-ray binaries. Among the remaining objects 36 are not firmly identified, due to the existence of multiple possible counterparts, and 11 are not associated to any likely counterpart. The HGPS paper is the most ambitious and comprehensive from the H.E.S.S. collaboration, and will act as the primary reference for the very-high-energy (VHE, ≥100 GeV) populations of the Galaxy until the CTA Galactic plane survey is published. In addition to the image and catalogue description, a systematic source association and identification procedure was performed and 16 new sources are described for the first time. Still, many questions concerning the birth, evolution and death of the cosmic particle accelerators that make up the Galactic TeV source population remain open. Progress in the next few years is expected to come from joint analyses with the Fermi-LAT space telescope (at GeV energies) and HAWC (at ~10 TeV) survey datasets, and comparisons to multi-wavelength surveys of the non-thermal radiation from the Milky Way, such as the anticipated eROSITA survey in the X-ray band.

The Galactic radiation field: A prerequisite for modelling the inverse Compton component of the γ-ray emission of the Milky Way is a knowledge of the distributions of interstellar radiation fields (ISRF) over wavelength and position throughout the Galaxy. In particular, the far-infrared component of the ISRF is the dominant source of seed photons giving rise to diffuse inverse Compton emission in the GeV-TeV range in photon energy, exceeding the contribution of the cosmic microwave background everywhere within the solar circle. Accordingly, the infrared astrophysics group at MPIK, in collaboration with the group of C. Popescu of the University of Central Lancashire (UK), has analysed archival COBE, IRAS and Planck maps of the near-IR to sub-millimetre emission of the Milky Way to obtain an improved solution for the diffuse interstellar radiation fields (ISRF) in the galaxy from UV to sub-millimetre wavelengths [1]. The analysis uses a modified version of the axisymmetric radiation transfer model developed for the analysis of external galaxies. This model is being adopted as a benchmark technique for the derivation of physical properties of galaxies from their panchromatic spectral energy distributions, in particular those

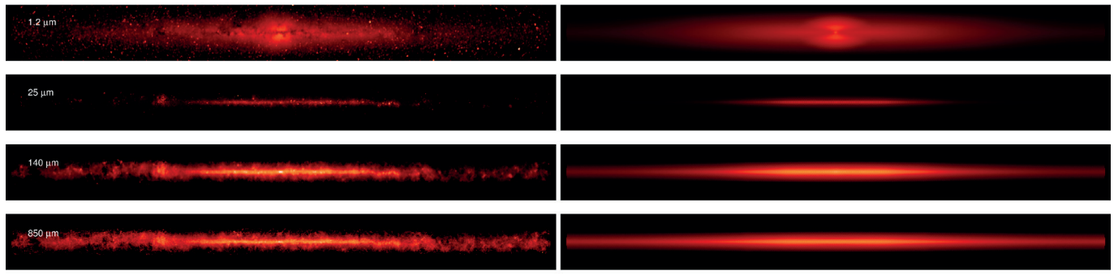

Fig. 2: Comparison of measured (left) and modelled (right) direct- and dust-reradiated starlight in the Milky Way, in a number of crucial bands (top to bottom: 1.2, 25, 140, 850 μm), indicating the good agreement on large scales.

spectral energy distributions made available through the Galaxy And Mass Assembly (GAMA) survey, in which the institute continues to actively participate. This approach to modelling the Milky Way enabled solutions to be found for the radial and vertical distributions of dust opacity and stellar emissivity which successfully predict the observed distributions of surface brightness of the Galaxy from NIR to sub-mm wavelengths (Fig. 2). As such, this is the first self-consistent model of the broad-band continuum emission from the Milky Way that predicts all available imaging observations. The solution for the ISRF provides an empirically rooted basis not only for the prediction of the inverse Compton γ-ray emission, but also for the pair-production opacity of the galaxy, which becomes significant towards the central regions at photon energies of tens of TeV.

Christoph Deil, Richard Tuffs

Propagation and Radiation of Relativistic Particles

Theoretical work is needed for the interpretation of observational data on the propagation and radiation of cosmic ray (CR) electrons and nuclei. A selection of the activities in this area over the last three years are summarised below.

Radiative processes: Considerable work has been done on improving parameterisations of γ-ray production in hadronic and leptonic interactions. In the case of inverse Compton scattering of electrons new analytical calculations have been performed for the case of single or combinations of blackbody (or graybody) radiation fields. The resulting energy spectra of up-scattered radiation and the rate of energy losses of electrons reach 1% level accuracy. The simple analytical functions derived are needed for the efficient fitting of models to measured spectral energy distributions, and are applicable for both isotropic and anisotropic target radiation fields.

Away from the γ-ray domain, but with important implications for electron accelerators, is work done on the polarisation properties of synchrotron radiation and jitter radiation (the analogue of synchrotron radiation in the case of highly non-uniform small-scale magnetic fields) in highly turbulent anisotropic magnetic fields. Such conditions may appear in relativistic shocks, in particular during the amplification of the magnetic field through the so-called Weibel instability. While the polarisation properties of the jitter radiation provide direct information on the turbulence spectrum as well as the geometry of magnetic field, the polarisation of the synchrotron radiation reflects the amplitude distribution of the magnetic field [2].

Cosmic-ray anisotropy: On the way from their source to the Earth, charged cosmic rays are deflected by the turbulent interstellar magnetic field. As a result, their angular distribution on arrival is almost isotropic, the amplitude of the anisotropy at TeV-PeV energies at Earth is about 0.1%, and, as expected, it is aligned with the direction of the local interstellar magnetic field. Until now, most theoretical studies assumed this large-scale anisotropy to have the form of a dipole. However, recent measurements using IceCube, IceTop and HAWC show anisotropy with highly significant deviations from a dipole structure.

One possible explanation lies in the simplistic assumptions frequently adopted when dealing with transport in a turbulent magnetic field. Therefore, explicit calculations of the CR anisotropy predicted for a range of theoretically motivated models of interstellar turbulence have been performed, and compared with data. The main findings are (i) the anisotropy is, in general, not a dipole, (ii) a range of models, in particular those that assume so-called "narrow resonance functions", are ruled out, and (iii) some models provide a good fit to the latest anisotropy data from the IceTop experiment. As an example, Fig. 3 shows the predicted anisotropy at around a PeV assuming "Goldreich-Sridhar" turbulence [3]. Both the observed shape and the energy dependence are well reproduced. This work demonstrates that the shape of the CR anisotropy encodes valuable information on the poorly known statistical properties of the local interstellar turbulence, and emphasises the potential of observational data to provide a quantitative probe.

Transition regime for cosmic-ray propagation: Cosmic-ray propagation is very often treated in the diffusive limit, even in cases where this approximation starts to break down, such as the transport of CRs very close to their sources. General analytical functions have

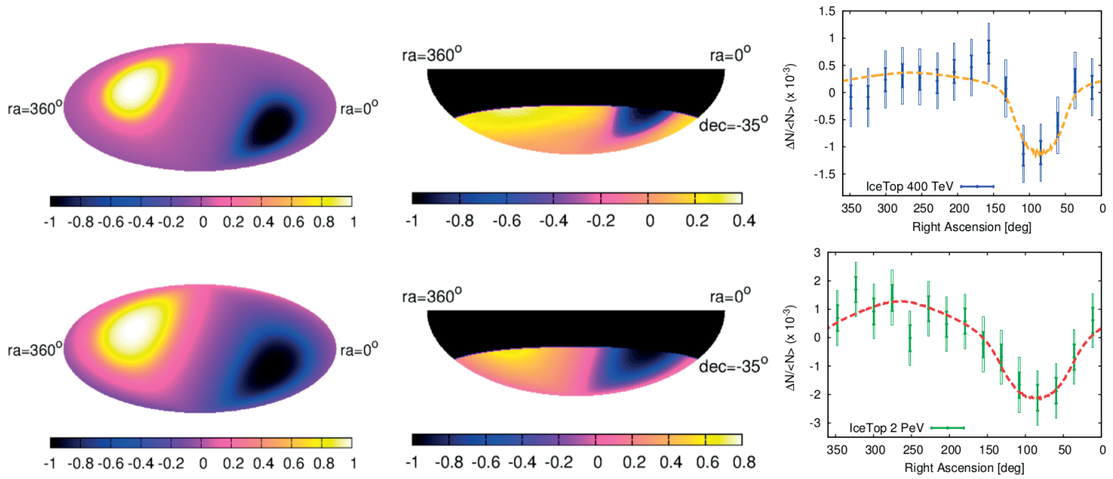

Fig. 3: A comparison of models to data on the anisotropy of the local cosmic-ray flux at around 400 TeV (upper row) and 2 PeV (lower row). Left: the normalised anisotropy in equatorial coordinates. Centre: the normalised prediction within the field of view of IceTop. Right: the predicted relative CR intensity as a function of right ascension, compared with IceTop measurements.

been derived for the angular, energy and radial distributions of cosmic rays outside of acceleration sites, including the transition between the ballistic and diffusion regimes [4]. Using these functions simulated γ-ray images have been produced, assuming the interaction of relativistic protons with gas clouds in the proximity of an accelerator. The morphology and the energy spectra of the γ-ray emission deviate significantly from the standard treatment of propagation of relativistic particles strictly in the diffusion regime.

Gwenael Giacinti, John Kirk, Anton Prosekin, Felix Aharonian

The Galactic Centre

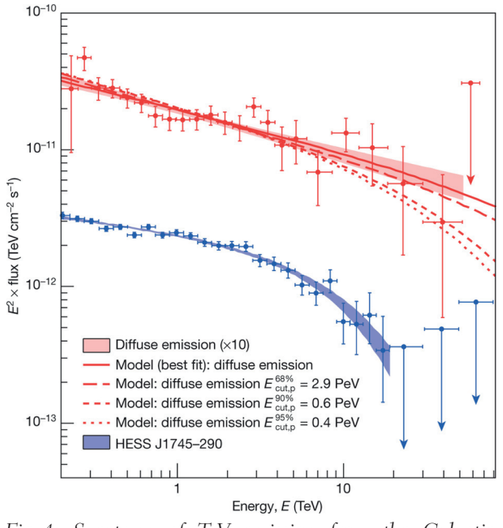

Fig. 4: Spectrum of TeV emission from the Galactic Centre: in blue the central point-like source (coincident with Sgr A) and in red the diffuse emission from the ~100 pc zone around the central source. No significant cut-off is seen in the spectrum indicating hadron acceleration up to ~PeV energies.*

The Galactic Centre (GC) region harbours a bright γ-ray source surrounded by a diffuse component of emission. While the central source coincides with the compact radio object Sgr A* – a suspected black hole at the dynamic centre of the Galaxy – the diffuse TeV γ-ray component is associated with the massive gas complex known as the Central Molecular Zone (CMZ). Although the diffuse component is undoubtedly caused by interactions of cosmic rays (relativistic protons and nuclei) with the dense gaseous complexes over the entire CMZ, the source of CRs (the accelerator) itself seems to be centrally located. This conclusion follows from the recent derivation of the radial distribution of CRs from H.E.S.S. γ-ray data and the spatial gas distribution in the CMZ [5], which show a 20-fold enhancement of the multi-TeV CR density near the GC, with the density falling off with distance as 1/r, as expected for CRs continuously injected and diffusing away from their source in interstellar magnetic fields. These findings suggest an association of the CR accelerator with Sgr A*, a promising candidate in terms of both energetics and acceleration arguments. The energy release through the accretion of the gas onto the black hole can proceed in different forms, in particular through acceleration of relativistic particles either in the immediate vicinity of the black hole (close to the event horizon) or at large distances from the central engine, e. g. at the termination of an outflow (a jet or a wind) that originates close to the black hole. The radial distribution of CRs indicates a quasi-continuous injection of CRs over the last ~1000 years. The spectrum of the diffuse γ-ray emission extends to energies well

above 20 TeV (see Fig. 4), and implies that the central source is a cosmic proton PeVatron (an object which accelerates protons to energies of ~1 PeV = 10^{15} eV): the first such object to be identified. The required injection rate of multi-TeV protons is uncertain due to the uncertain diffusion speed and resulting confinement time in the CMZ, but clearly exceeds the current bolometric luminosity of electromagnetic radiation of Sgr A*, and constitutes a non-negligible fraction of the current accretion power of the central super-massive black hole. This particle accelerator alone could account for most of the flux of Galactic CRs around the so-called "knee" of the CR spectrum at energies of a few PeV, if its power, at least over the last ~10^6 years, has been maintained at the average level of 10^{39} erg/s above 10 TeV. Moreover, the escape of these particles into the Galactic halo and their subsequent interactions with the surrounding gas may be responsible for the sub-PeV neutrinos recently reported by the IceCube collaboration.

At much lower γ-ray energies the diffuse emission of the GC region and the wider Galaxy has been explored using data from the Fermi Large Area Telescope (LAT). These data show that the CR density in the inner Galaxy substantially exceeds the density in the outer Galaxy, supporting the idea that the GC region is playing a major role in CR acceleration in the Milky Way [6].

Felix Aharonian, Aion Viana

Supernova Remnants as a Source of Cosmic Rays

Supernova remnants (SNRs) have long been suspected to be the dominant source of the Galactic cosmic rays. Only very recently has this picture started to be confirmed experimentally, but a number of major puzzles remain, including the maximum energy to which these objects can accelerate and the way in which particles propagate out of their sources and to the Earth. Work on the γ-ray emission of SNRs at the MPIK has involved placing constraints on the population of Galactic SNRs using the HGPS data discussed above, but also targeting important individual objects, two of which are discussed below.

Of all γ-ray emitting SNRs, RX J1713-3946 is perhaps the best known, being the first source ever resolved in γ rays and one of the brightest TeV emitters in the sky. The H.E.S.S. collaboration has regularly observed this "old friend" for a period of almost 10 years resulting in an extremely large (164 hour) dataset. Such a large dataset, combined with newly developed analysis techniques, allow the remnant to be studied in unprecedented detail [7]. The morphology of RX J1713-3946 in the TeV range can now be compared in detail to that observed at lower energies. Fig. 5 shows in particular a comparison of the radial profile of the H.E.S.S. emission with that seen by the XMM-Newton X-ray telescope. The SNR as seen at TeV energies extends beyond the shell seen in X-rays. Such an effect has in the past been predicted by diffusive shock acceleration theory, with the X-rays marking the edge of the shock region and the TeV emission highlighting particles either in the precursor region of the shock, or completely escaping from it. Although it is, as yet, not possible to distinguish between these scenarios, this is the first direct observation of accelerated particles in the process of leaving the shock region of an SNR, and supporting the idea that cosmic rays with energies of 100s of TeV can only be accelerated, and confined within, very young SNRs.

W49B is another object of particular interest in the hunt for the origin of the Galactic cosmic rays. It is another rather young SNR (~2000 years), but with clear evidence that its shock front is interacting with dense molecular material, potentially enhancing γ-ray emission via hadronic processes. This object was detected using both H.E.S.S. and Fermi-LAT,

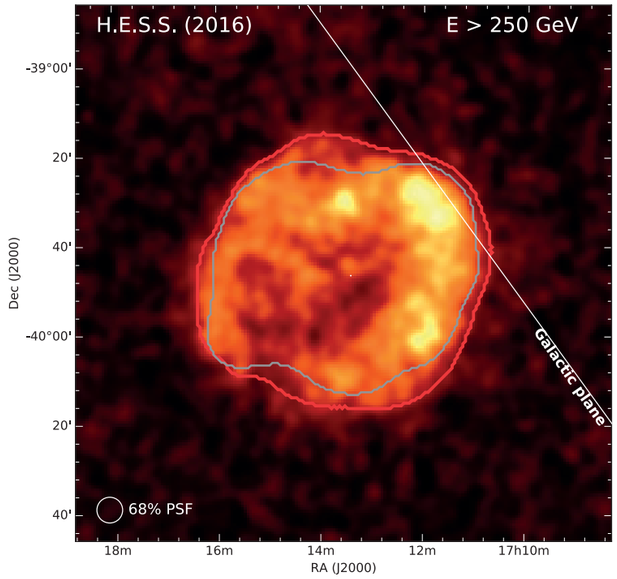

Fig. 5: The supernova remnant RX J1713-3946 in >250 GeV γ rays from the latest H.E.S.S. data. The outer edge of the TeV emission (red contour) is compared to that of the X-ray emission measured with XMM-Newton (gray contour).

allowing a joint analysis of the emission spectrum, which shows some interesting features. At low energies a spectral break is seen, similar to those detected in other interacting SNRs (IC 443, W44 and W51C) and is typically interpreted as the signature of γ-ray emission produced through neutral-pion decay. Additionally, the joint spectral fit reveals a second spectral break at 8.4 GeV, similar to those observed in other SNR/molecular cloud associations. When comparing these results with model predictions, both hadronic and leptonic emission scenarios can explain the measured spectral shape, but the low-energy break favours the hadronic interpretation. W49B therefore joins the small club of SNRs where there is now convincing evidence of acceleration of hadronic cosmic rays [8].

Dan Parsons, Vincent Marandon

Pulsar Wind Nebulae

Pulsars – rapidly rotating, strongly magnetised neutron stars – are known to power the compact clouds of relativistic, magnetised, electron-positron plasma that surround them (Pulsar Wind Nebulae: PWN) and that make up the majority of the Galactic sources so far identified at TeV energies. Energisation of the radiating particles is thought to occur when the extremely low-density relativistic wind from the pulsar terminates on hitting the surrounding medium. It seems, however, that the acceleration mechanism at work here must differ significantly from those studied in other astrophysical contexts, such as supernova remnants. On the one hand, unlike SNR, pulsar winds contain a magnetised, relativistic plasma, which permits the propagation of low frequency electromagnetic waves. On the other hand, observations imply that the spectrum of accelerated particles is substantially different to that found in SNR.

Acceleration processes: Continuing a series of investigations on this topic, the acceleration process at pulsar wind termination shocks has been studied using the complementary numerical techniques of two-fluid simulation, test-particle trajectory integration and Monte-Carlo simulation [9]. These investigations show that the shock is characterised by an electromagnetic precursor, in which low-frequency, electromagnetic waves dissipate and accelerate the incoming particles. In the equatorial parts of the wind, the pulsar's magnetic field is completely annihilated by this structure, which reflects roughly 10% of the incoming particles, and accelerates both these and the transmitted particles into a distribution similar to a relativistic Maxwellian. Monte-Carlo simulations were used to follow up on the fate of the reflected particles, and showed that they are further accelerated into a scale-free power-law distribution, with a spectral index similar to that predicted for un-magnetised, relativistic MHD-shocks, thereby providing a viable explanation of the high-energy spectrum observed from the Crab Nebula.

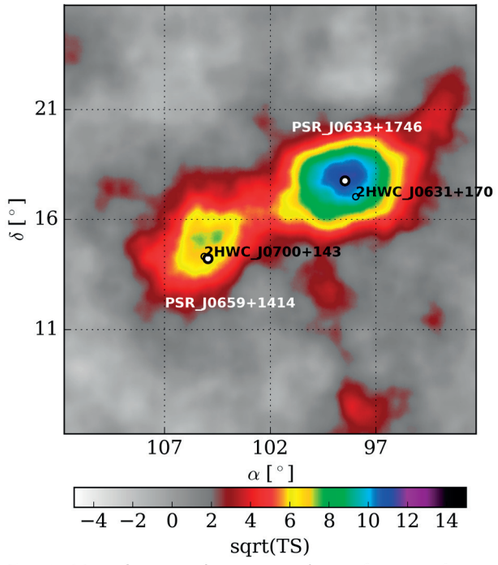

Fig. 6: Map showing the statistical significance of γ-ray emission from one year of HAWC data from a search for extended emission. Two sources are apparent: extended emission nebulae around the two very nearby pulsars PSR J0659+14 and Geminga.

Gamma-ray observations: Observationally the focus has been on prominent bright and nearby γ-ray emitting PWN, in an attempt to understand the propagation of relativistic particles in the extended nebulae well beyond the termination shock. With H.E.S.S. we have continued to study the archetypal middle aged (~20 000 year old) PWN HESS J1825-137. With a larger dataset, including observations with the five-telescope H.E.S.S.-II system, and improved analysis methods, the energy-dependent morphology of the system can be studied in much greater detail. The γ-ray nebula shrinks with increasing energy, very likely due to the more rapid energy losses of higher energy electrons in the nebula. From the way in which the emission changes with energy, particle transport inside the nebula can be constrained, favouring advection over diffusion as the dominant mechanism [9].

For closer and older systems than HESS J1825-137 the field of view of H.E.S.S. starts to be a limiting factor and a wide-field detector such as HAWC comes in to its own. Very recently [10] extended γ-ray emission has been detected with HAWC around two local pulsars: Geminga and PSR J0659+14. The analysis and interpretation of these data has been a major recent activity at MPIK. The >4° diameter emission around these old and low-power systems (see Fig. 6) suggests that the radiating electrons occupy a volume much larger in that within which the pulsar dominates the interstellar medium (ISM). This would be the first γ-ray measurement of cosmic-ray electrons diffusing away from an identified source into the ISM. These measurements allow the contribution of these objects to the locally measured cosmic-ray electron (and positron) flux to be constrained and will provide insights on relativistic particle propagation in general.

Simone Giacchè, John Kirk, Alison Mitchell, Rubén López Coto

Binary Systems

Binary systems have been established in the last ~10 years as a distinct class of variable, high-energy (HE, 0.1-100 GeV) and VHE γ-ray emitters. The MPIK has been a major contributor to the advances in our understanding of this rich and varied category of cosmic particle accelerators over the last three years. Results include the identification of new γ-ray binary systems with H.E.S.S. and the Fermi-LAT satellite, follow-up observations in other wavebands and the modelling and interpretation of the mechanisms responsible for their γ-ray emission.

Microquasars: X-ray binaries displaying relativistic jets are known as microquasars, in analogy to the black-hole powered quasars. Gamma-ray emission from these objects was long predicted, but only recently confirmed observationally.

Cyg X-3 was the first undisputed γ-ray emitting microquasar, established through Fermi-LAT and AGILE observations. Recently, two other well-known microquasars at γ-ray energies were detected, Cyg X-1 and SS 433, from the analysis of archival Fermi-LAT data. In the case of Cyg X-1, the source is detected only during the so-called hard states, when a relativistic jet is present, with higher fluxes during orbital phases close to the superior conjunction of the binary system, suggesting that γ rays are produced through anisotropic IC emission and placing the γ-ray emitter close to the black hole, ~10^{11}-10^{12} cm [11]. In the case of SS 433 the emission is restricted to energies below 800 MeV, with a distinct spectral maximum at ~250 MeV. No significant variability is found in the data, suggesting that γ rays could be produced in the jet/medium interaction regions.

VHE γ-ray binaries: the class of binary systems with significant TeV emission are thought to be associated with pulsars, i. e. compactified pulsar wind nebulae inside high mass binary systems. Only four systems of this class are well-established, but two new strong candidates have emerged very recently, with the MPIK playing a major role. H.E.S.S.-II observations of the established short-period system LS 5039 have allowed its spectrum to be connected between the GeV and TeV domains and established a 'swiss-clock'-like regularity of the orbitally-modulated VHE emission over more than a decade. The much longer period system PSR B1259-63 is subject to dramatic variability around periastron passage, with H.E.S.S. observations indicating a high VHE flux level at the time of a HE flare during the 2014 periastron. This flaring behaviour may be associated to inverse Compton emission in the un-shocked pulsar wind region.

The two new γ-ray binaries candidates are 1FGLJ1018.6–5856 and HESS J1832–093. The former was initially discovered using Fermi-LAT, and a VHE counterpart detected in follow-up observations with H.E.S.S. When folded on the system's orbital period of ~16.6 days the light-curve peaks in phase with the observed X-ray and HE emission, contrary to the otherwise similar system LS 5039. HESS J1832–093 was an unidentified point-like source in the Galactic plane discovered using H.E.S.S., triggering X-ray observations with XMM-Newton in which a hard, highly absorbed X-ray point source counterpart was detected. Recently, deep follow-up observations in X-rays with Chandra and Swift were performed. These observations show dramatic X-ray variability and pin-point the source to an infrared counterpart which is believed to be the stellar companion [12].

Colliding wind binaries: The colliding wind binary system (CWB) η-Carina is characterised by displaying extremely powerful winds, and is the only CWB so far detected at γ-ray energies. We have worked on time-dependent modelling of the non-thermal emission,

confirming that efficient hadron acceleration is very likely taking place, and that the two distinct high-energy components are a natural consequence of the two shocks on either side of the contact discontinuity in this system. H.E.S.S.-II observations of η-Carina are on-going and will allow us to tightly constrain acceleration to high energies in this system.

Pol Bordas, Roberta Zanin, Jim Hinton

The Large Magellanic Cloud

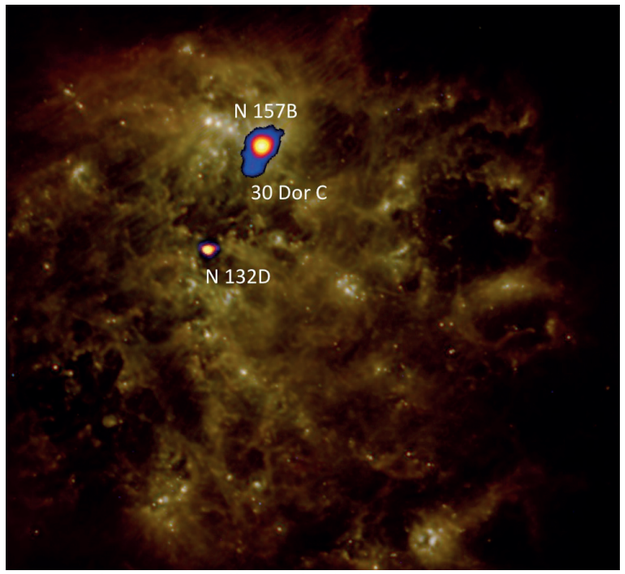

Fig. 7: In the Large Magellanic Cloud, three TeV sources are apparent, coincident with a powerful pulsar (N157B), a young supernova remnant (N132D), and the exceptional star-forming region 30 Doradus C.

As one of our closest galactic neighbours (at only 50 kpc) the Large Magellanic Cloud (LMC) is an extremely interesting target for VHE γ-ray observations, as it allows us to study the same source classes seen within our own galaxy, but within a different galactic environment, and with a face-on view. Over the lifetime of H.E.S.S. around 200 hours of observation time have been dedicated to the study of this region, resulting in the detection of three new γ-ray sources of different classes [13]. Fig. 7 shows these three new sources in the context of the LMC. Two of the sources, N157B and N132D, are exceptionally energetic examples of already known galactic source classes, supernova remnants and pulsar wind nebulae, respectively. The third source, 30 Doradus C, part of the massive star-forming region, the "Tarantula Nebula", represents an entirely new source class.

The "superbubble" 30 Dor C is the largest non-thermal X-ray emitting shell yet found and appears to have been created by the collective effects of several supernovae and strong stellar winds. Such superbubbles have been suggested as potential sites of cosmic-ray acceleration. The H.E.S.S. detection of 30 Dor C confirms the presence and production of energetic cosmic rays within this source class.

Finally, and quite surprisingly, no TeV emission is yet seen from the recent supernova SN 1987A, placing constraints on the acceleration of particles in very young supernova remnants. Further observations of the LMC are being made with the improved sensitivity of the H.E.S.S.-II array, which will allow for a deeper study of the TeV source population. Looking further ahead, the MPIK group is involved with the planning of a CTA Key Science Project surveying the LMC and expected to reveal diffuse emission as well as source populations which will provide an important complement to the survey of our own galaxy.

Dan Parsons, Pol Bordas

Active Galactic Nuclei

Active Galactic Nuclei (AGN) host accreting supermassive black hole systems that produce collimated relativistic outflows ("jets") and thereby facilitate the transport of energy over huge scales. Particle acceleration in AGN is a long-standing research topic at the MPIK and in the last few years detailed studies of two very different objects have provided substantial insights into source physics and plasma characteristics of AGN. Here two results are summarised, involving the luminous blazar (a system with one jet aligned very close to the line of sight) PKS 2155-304 (at a distance of ~500 Mpc) and the nearest radio galaxy Centaurus A (at ~4 Mpc).

Cen A is known for its complex morphology that ranges from sub-pc jet features to giant radio lobes on ~100 kpc scales. Recent work based on an analysis of high-energy (HE, >100 MeV) Fermi-LAT data along with low-energy (30-900 GHz) Planck data reveals the detailed morphology of the giant lobes at radio and γ-ray energies (see Fig 8). The larger HE dataset allows the spectrum of the lobes to be extended up to 30 GeV and down to 60 MeV, while inclusion of Planck data made it possible to put stringent constraints on the cut-off region of the synchrotron-emitting electrons. These results imply that the low-energy γ rays must be of leptonic origin (electron inverse Compton up-scattering of CMB photons) raising questions about in-situ particle acceleration, while hadronic (pion-decay) emission may contribute to the high-energy γ-ray tail, with important implications for the jet power and nuclear activity in Cen A [14]. On smaller angular scales (<5 kpc), we find an unusual spectral hardening ("upturn") of the HE "core" spectrum in Cen A at energies of a few GeV, triggering many new investigations. Analysis of new H.E.S.S. observations indicates that the new HE component can be smoothly connected to the emission seen at TeV energies. CTA is likely needed to resolve the origin of the two emission components in the core.

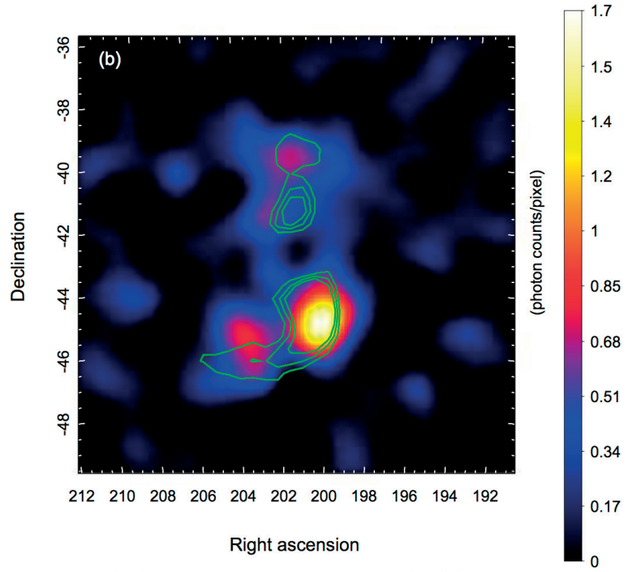

Fig. 8: Residual map of γ-ray emission from the lobes of Centaurus A from Fermi-LAT after the subtraction of diffuse background emission. Green contours show 30 GHz emission measured by the Planck satellite.

In contrast to Cen A, PKS 2155-304 is a bright γ-ray source, allowing for a detailed variability analysis of its emission beyond minimum variability considerations. New results show that the observed emission can in general be characterised as power-law noise, where the index at very high energies (VHE, >100 GeV) is similar to that at HE, yet seemingly different for active and quiescent source states. The finding that the observed fluxes follow a log-normal distribution implies that the underlying physical process shaping the emission must be multiplicative. This offers important physical insights and could be interpreted as evidence for a disk origin of its jet. PKS 2155-304 is currently emerging as the prototypical source for applying time-domain astronomy techniques to γ-ray data, with huge potential for progress in the understanding of these enigmatic objects.

Frank Rieger, Felix Aharonian, Ruizhi Yang

References:

[1] C.C. Popescu, R. Yang, R.J. Tuffs et al., Monthly Notices Royal Astron. Soc., accepted
[2] A. Prosekin, S.R. Kelner, F.A. Aharonian, Phys. Rev. D, 94, 063010 (2016)
[3] G. Giacinti, J.G. Kirk, submitted to the Astrophysical Journal (arXiv:1610.06134)
[4] A.Y. Prosekin, S.R. Kelner, F.A. Aharonian, Phys. Rev. D 92, 083003 (2015)
[5] H.E.S.S. Collaboration, Nature 531, 476 (2016)
[6] R. Yang, F.A. Aharonian, C. Evoli, Astronomy & Astrophysics 589, A117 (2016)
[7] H.E.S.S. Collaboration, Astronomy & Astrophysics, accepted (arXiv:1609.08671)
[8] H.E.S.S. Collaboration, Astronomy & Astrophysics, accepted (arXiv:1609.00600)
[9] S. Giacchè, J.G. Kirk, Astrophysical Journal, accepted (arXiv:1612.04282)
[10] A. Mitchell et al, Proceedings of the Heidelberg Gamma-ray Symposium 2016
[11] R. Lopez Coto et al, Proceedings of the Heidelberg Gamma-ray Symposium 2016
[12] R. Zanin et al, Astronomy & Astrophysics 596, A55 (2016)
[13] P. Eger et al., Monthly Notices Royal Astron. Soc. 457, 2, 1753 (2016)
[14] H.E.S.S. Collaboration, Science, 347, 406 (2015)
[15] X. Sun, R. Yang, B. Mckinley, F.A. Aharonian, Astronomy & Astrophysics, 595, A29 (2016)

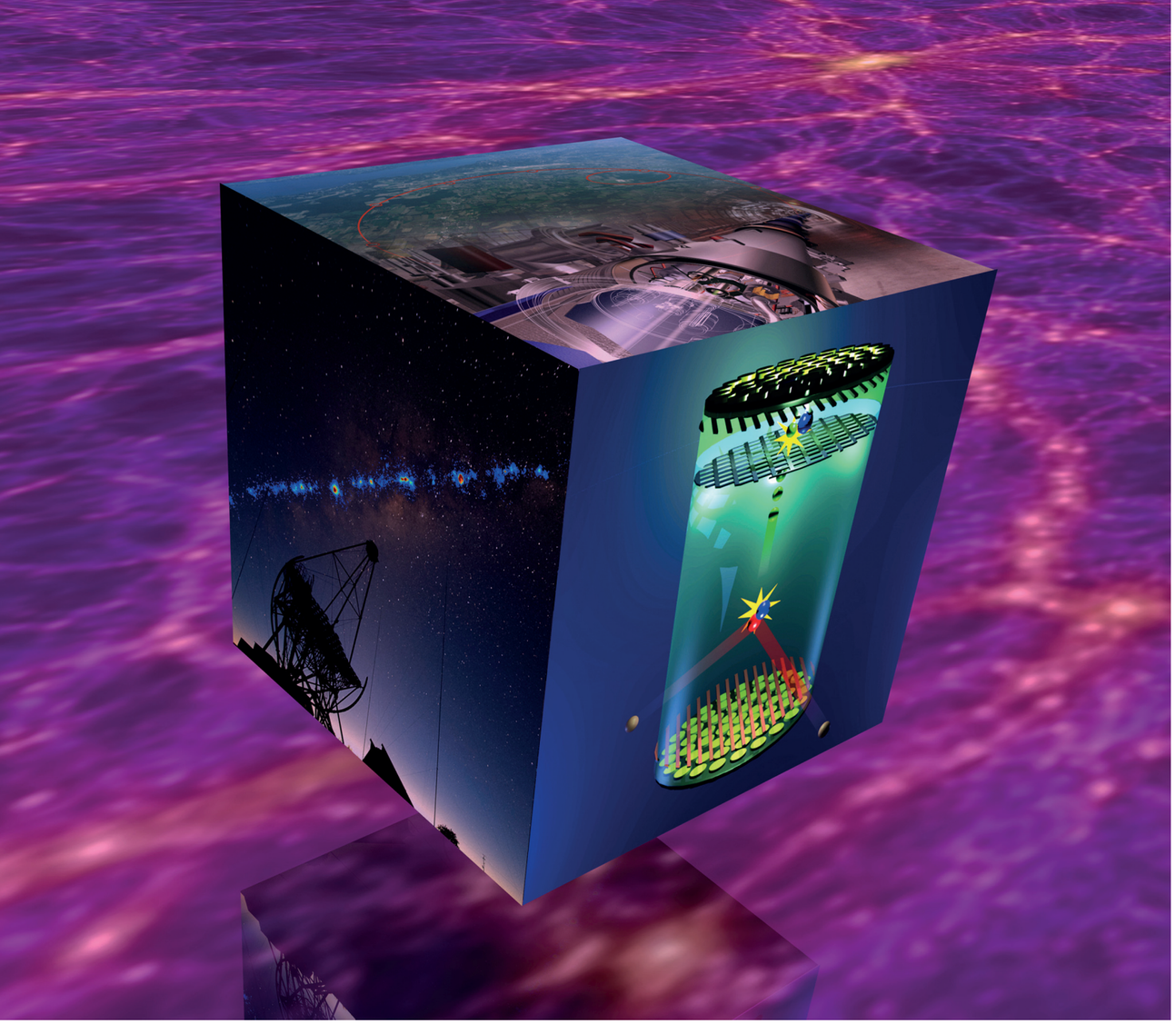

1.3 Dark Matter

Complementarity searches for dark matter: direct, indirect and collider (image: CERN). Background: the network of dark matter according to the millennium simulation (MPI for Astrophysics).

Introduction

One of the biggest open questions in today's particle physics and cosmology is the identification of the Dark Matter (DM) in the Universe. A large collection of cosmological as well as astrophysical observations show strong evidence that a large fraction of the matter in the Universe cannot be made out of the known forms of matter, consisting of protons, neutrons, and electrons. Extensions of the Standard Model of particle physics, which are anyway required for other reasons, contain often so-called Weakly Interacting Massive Particles (WIMPs) which are ideal Dark Matter candidates. Their properties imply that the right magnitude of Dark Matter was automatically produced in the Big Bang and they also fit to all other indirect astronomical and cosmological evidences.

Dark Matter Theory and Phenomenology

The existence of dark matter (DM) has been established, via its gravitational effects, through a variety of observations at different scales from galaxies to the largest structures in the Universe. According to the most recent cosmological data, DM accounts for about 27% of the total energy density of the Universe and about 85% of its matter density. And yet, the fundamental nature of the DM particle (e.g. its mass, spin, quantum numbers, etc.) remains a mystery, providing one of the most important open problems in particle and astroparticle physics today. There are several candidates for dark matter and some of the most compelling are weakly interacting massive particles (WIMPs) and sterile neutrinos.

WIMPs are stable particles and are related to fundamental problems in particle physics. The standard model of particle physics that offers a unified description of strong and electroweak forces is plagued with the so-called hierarchy problem. In simple terms, it means that if there is new physics at an energy scale larger than the weak scale, the theory has to be exceedingly fine-tuned in order to cancel divergent quantum contributions and keep the mass of the Higgs boson at the observed value of 126 GeV. There are ways to circumvent this issue, and a prominent solution is supersymmetry, which naturally predicts the existence of WIMPs. A distinct feature of WIMPs is that they generally reproduce the right relic dark matter density of the universe through a processes known as thermal freeze-out, as result of their interaction strength being at the weak scale. Regardless of the quantum numbers, these WIMPs are capable of yielding the right amount of dark matter, while producing signal within reach of current and planned direct and indirect detection experiments. These unique elements make WIMPs prominent dark matter candidates.

Albeit, in order to pin down the properties of the WIMPs one needs to combine data from different search strategies, namely direct, indirect and collider searches [1].

Direct detection searches probe the WIMP-nucleon scatterings, indirect detection the annihilation cross section into cosmic rays, gamma rays and neutrinos, while collider experiments its production rate induced by the production of unstable new particles. MPIK has been involved in experimental searches for dark matter using gamma rays and neutrinos [2] and in direct and indirect detection to probe new physics models [3, 4].

A promising approach to probe WIMP models is to take advantage of their distinct features such as the possible emission of gamma-ray lines, which is a clear signature to

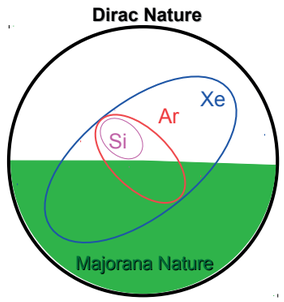

Fig. 1: Nature of dark matter.

establish the presence of WIMPs annihilations in our galaxy. However, such line emissions are highly constrained by gamma-ray telescopes. An interesting fact is that direct detection experiments such as XENON1T or XENONnT should see at some level a WIMP signal. This expectation rests on the observation that a WIMP of mass m has classically a size 1/m set by the De Broglie wavelength. Multiplying the resulting area with a weak coupling or a Higgs portal coupling and a model-dependent factor typically O(1, ..., 0.001) one ends up with spin-independent (SI) cross sections in the range between 10^{-44} cm^2 to 10^{-49} cm^2. This explains, for example, also the cross section range for the MSSM as can be seen in the framework of the MSSM in [3]. This is very interesting, since this range is already partly probed and will to a large extend be fully probed in the coming years by XENON1T or XENONnT. However, it is rather difficult to unveil the fundamental nature of the WIMPs, in other words, determine if they are Dirac or Majorana fermions, real scalar or complex scalar for instance (see Fig. 1). Therefore, a test capable of distinguishing the dark matter particle from its anti-particle was proposed [4], with the XENONnT experiment playing a key role. With the observation of three signals originated from WIMP-nucleon spin-independent scatterings in xenon, silicon, and argon nuclei, a test can be constructed to possibly establish the Dirac nature of dark matter, for instance. In summary, the next decade will be crucial to test the WIMP paradigm.

Albeit, as aforementioned, dark matter might as well be formed of sterile neutrinos, and in this case the picture changes dramatically. Sterile neutrinos are well-motivated candidates because they are tightly connected to neutrino masses. Since keV sterile neutrinos are expected to mix with active neutrinos, they decay producing a keV line, and that has been the smoking gun signature for sterile neutrinos. Excitingly a 3.5 keV X-ray line emission was observed both in a stack of galaxy clusters and in the Galactic Centre, and that was immediately interpreted as hint for sterile neutrinos. Some works questioned the origin of this X-ray line later on, so at this point its origin is unclear. Be that as it may, sterile neutrinos are among the most popular dark matter candidates. Thus one may wonder, what are the other possible observable signals for warm dark matter sterile neutrinos? In [5], for the first in the literature, we tried to answer that fundamental question. In particular, if keV sterile neutrinos scatter inelastically with bound electrons of the target material, an electron recoil signal is generated. Therefore, one can search for sterile neutrino warm dark matter through direct detection experiments, such as XENON100, XENON1T and DARWIN. In [5] the first direct laboratory bounds on sterile neutrino warm dark matter were derived (see Fig. 2) as a function of mixing angles and sterile neutrino mass. While not necessarily as stringent as astrophysical probes, they provide complementary and competitive limits, and their results paved the way for a new search strategy for sterile neutrinos as dark matter candidates.

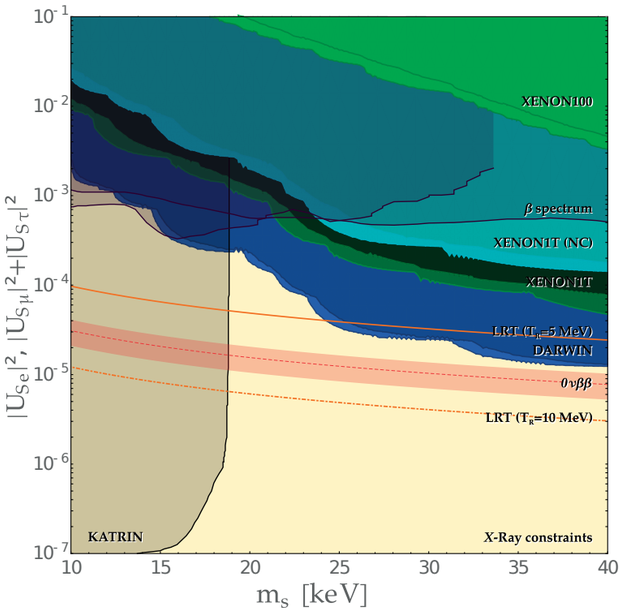

Fig. 2: Search for sterile neutrinos with direct detection experiments.

Many other theoretical and phenomenological aspects of dark matter were studied at MPIK in the reporting period, resulting in close to 50 publications. A short list of examples: Various models for dark matter and possibilities to constrain its properties were studied. This usually reveals connections to collider, lepton or neutrino physics. For instance, if the dark matter particle belongs to a new class of interactions, additional particles are predicted. Natural examples are gauging the difference of baryon and lepton number, or the difference of the leptonic muon and tau flavours. Here new gauge bosons are predicted, which can be produced at colliders, or can be seen indirectly via their contribution to the anomalous magnetic moment of the muon. Gauging the baryon or lepton number individually implies the existence of new fermions with exotic quantum numbers. Extending the additional interactions further leads for instance to left-right symmetric theories. Adding here a new multiplet allows to have a stable dark matter candidate, where the stability is either accidental or from a remaining discrete symmetry after the breaking of the left-right symmetry. Other models that have been studied imply a dark matter candidate that is involved in the radiative generation of neutrino mass. Other connections appear in models in which additional inert Higgs doublets (i. e. not coupling to Standard Model fields) are dark matter particles and are involved, together with new quarks, in the Peccei-Quinn solution of the strong CP problem. Such scenarios involve even the possibility of the coexistence of WIMP and axion dark matter. Moreover, so-called scale-invariant models were considered, in which masses arise from radiative breaking of a conformal symmetry. Dark matter particles can easily be incorporated in such scenarios.

Turning to phenomenology, one can note that if the dark matter interactions with matter are isospin-violating (i. e. different coupling to protons and neutrons), the comparison of different direct detection experiments is different from the standard case. It is possible to suppress the direct detection sensitivity of experiments using xenon, which in the standard case are expected to provide the strongest constraints. Global continuous symmetries invoked to stabilise the dark matter are expected to be broken by gravity effects. Thus, dark matter will eventually decay in such scenarios. By considering gravitational interactions, lifetime limits on several dark matter candidates can then be obtained.

If the dark matter particle couples to Standard Model particles, one expects that via loop processes gamma-ray lines are generated, and the predictions need to be confronted with observational H.E.S.S. and future CTA constraints, see below. Interestingly, if the dark matter annihilates in neutrinos, a gamma-ray spectrum generated by electroweak bremsstrahlung is always produced as well. For dark matter masses above 200 GeV, gamma-ray data actually set the most stringent constraints on neutrino lines from dark matter annihilation and, therefore, an upper bound on the dark matter total annihilation cross section.

Farinaldo da Silva Queiroz, Werner Rodejohann, Manfred Lindner

XENON100 and XENON1T

In the past decades various detector technologies have been developed with the goal of directly detecting dark matter interactions proving, eventually, the answer to one of the most important open question in modern physics. The XENON100 experiment, located at the Gran Sasso underground laboratory (LNGS), has set over the last years most stringent upper limits on the interaction cross section of dark matter with known matter. The detector consists of a two-phase liquid-xenon time projection chamber (TPC, see title image, right) equipped with two arrays of photomultiplier tubes which detect efficiently tiny signals (only a few photons). The combination of two signals: from scintillation photons (S1) and from charges drifted to the gas phase (S2) allows to reconstruct the event position in three dimensions and gives a separation between common background originated by γ and β particles and the expected nuclear recoil signal. The high stopping power of liquid xenon together with the choice of radio-purest materials for the detector, and a passive shield towards environmental radiation results in a detector with one of the lowest interaction rates ever measured.

XENON100 has acquired science data since 2009. Several physics results have been derived from the second major run of 225 live days data. Beside the standard WIMP interpretation of the data, we have investigated other possibilities in which a dark matter candidate interacts with electrons. With no evidence for a signal above the low background of our experiment, we placed limits on axion models and also on leptophilic dark matter candidates [6]. Furthermore, motivated by the annual modulation of the signal observed by the DAMA experiment, we studied if such signature is present in our detector. Following a detailed study to establish the stability of the detector and its background contributions, we searched for periodic variations of the electronic recoil event rate. As the data suggested no statistically significant modulation, we exclude the DAMA/LIBRA signal interpreted as a dark matter signature with axial-vector coupling of WIMPs to electrons at 4.8 sigma.

The final WIMP search results of the XENON100 experiment [7] have been released in 2016, these combine three individual runs summing up to 477 live days with data taken between January 2010 and January 2014. Data from the first two runs had already been published. A stable performance of the photomultiplier tubes, cryogenic, purification system, electric field configuration over several years enables a combination of the runs with minimal changes in the treatment of data. The ultra-low electromagnetic background of the experiment, $\sim 5 \times 10^{-3}$ events/($\mathrm{keV_{ee}} \cdot \mathrm{kg} \cdot \mathrm{day}$) before electronic recoil rejection, together

with the increased exposure of 48 kg·y improves the sensitivity. Systematic uncertainties are reduced by an improved background modelling, a more robust usage of the derived light collection efficiency and by exploiting both energy scales of the scintillation and charge signal in the computed signal model. A profile likelihood analysis using a common energy range of (6.6-43.3) keV_{nr} for all three runs sets a limit on the elastic, spin-independent WIMP-nucleon scattering cross section for WIMP masses above 8 GeV/c^2, with a minimum of 1.1×10^{-45} cm^2 at 50 GeV/c^2 and 90% confidence level. In addition, the constraints on the elastic spin-dependent WIMP-nucleon cross sections obtained with the same data were updated.

Fig. 3: The XENON1T experiment. On the left the water tank containing the xenon cryostat and on the right the service building with various auxiliary systems.

To significantly increase the sensitivity with respect to XENON100, a next generation, the XENON1T experiment [8], has been built also at LNGS (see Fig. 3). The detector construction started at LNGS in summer 2013 and the detector was commissioned between 2015 and early 2016. With a target mass 32 times larger than XENON100 and a reduced background rate, the sensitivity to the spin-independent WIMP-nucleon interaction cross section is expected to reach two orders of magnitude down in cross sections compared to the current XENON100 results (see Fig. 4).

With around 1.5 tons of xenon, MPIK has contributed almost half of XENON1T's required xenon mass of 3.3 tons. Furthermore, we took responsibility of transferring the gas from the purchased bottles to the storage vessel at LNGS and ensuring a high gas purity. Using a customised gas chromatography setup that was optimised in cooperation with the supplier, the entire xenon inventory of XENON1T was measured for contaminations. With its sensitivity of tens of ppb (parts per billion) for the relevant trace impurities, it was possible to identify contaminated xenon bottles before their content would be mixed with the rest high-purity xenon. Rejected xenon bottles were purified in dedicated cryogenic distillation campaigns. Combining all the measurements, the nominal krypton and oxygen contaminations of the XENON1T's xenon inventory were below 25 ppb and 55 ppb, respectively.

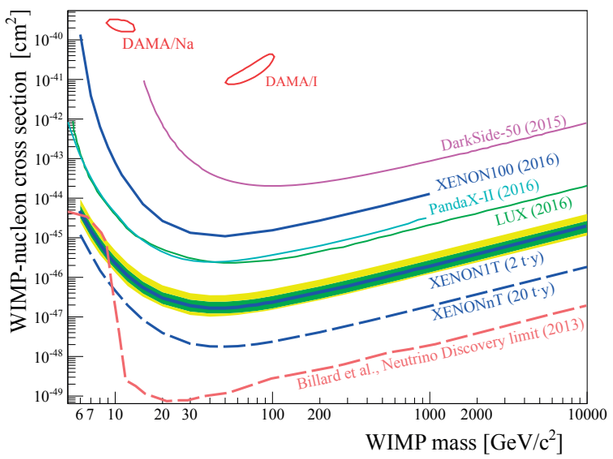

Fig. 4: XENON1T and XENONnT sensitivity (90% C.L.) to spin-independent WIMP-nucleon interaction.

Due to the presence of the anthropogenic radionuclide ^{85}Kr in the atmosphere, the concentration of natural krypton in xenon has to be reduced to 0.2 parts per trillion (ppt) [8] to achieve the low background required for XENON1T. For this ambitious goal a dedicated distillation column has been constructed by the XENON1T collaboration. Design and development of this device was strongly supported by an analytical tool developed, maintained and

operated at MPIK. The rare-gas mass spectrometer (RGMS) combines a gas chromatographic separation of krypton traces from the bulk xenon and a sector-field mass spectrometer to quantify these traces. The RGMS achieves a detection limit of 0.008 ppt [9], more than an order below the requirements for XENON1T, and verified the excellent performance of the XENON1T distillation column. After its final installation at the XENON1T experiment, a Kr/Xe concentration below 0.056 ppt (95% C.L.) was measured. Further, the RGMS is heavily employed to monitor the evolution of the krypton concentration in XENON1T. Based on the frequent and fast feedback of this device, an online purification scheme was devised to reduce the krypton level in parallel to operating the XENON1T detector increasing thereby the duty-cycle of the experiment.

The chemically inert noble gas radon presents another challenging background source in liquid xenon detectors. It is emanated by the construction materials and distributes in the detector. Therefore, a careful material selection of all employed detector components is required. For this purpose not only the world's most sensitive GeMPI Germanium spectrometres located at LNGS are employed, but also a dedicated radon emanation screening setup developed at MPIK. It is based on miniaturised proportional devices with an ultra low detection limit that count alpha disintegrations subsequent to the radon decays. Before and during the building phase of the XENON1T detector, the emanation measurements were mostly performed locally at the MPIK. Measurements of bigger detector parts and combined sub-systems were directly realised on the construction site at LNGS. By selecting materials with a low radon emanation rate, we achieved a reduction of a factor of 5 in XENON1T with respect to XENON100. Nevertheless, the emanation measurements showed that radon will be the main intrinsic background in XENON1T. This knowledge is important for the data analysis in which the MPIK is involved, and serves as a crucial input for the prediction of the electronic recoil background in XENON1T.

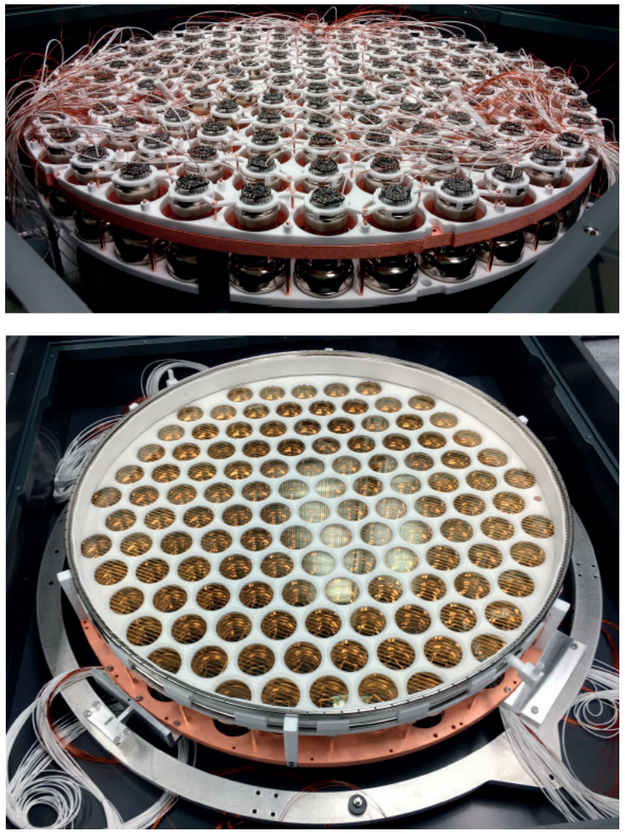

Fig. 5: Photographs of the PMT arrays of XENON1T.

The TPC of XENON1T has about 1 m length and 1 m diameter and it is also equipped with two arrays of photosensors. Together with the company Hamamatsu, we have developed a photomultiplier optimised for a very low intrinsic radioactivity [10], a high quantum efficiency and a high sensitivity to single photon detection. A total of 248 tubes are currently operated in XENON1T, selected out of 321 tested units. All tubes were tested at MPIK at room temperature and also in a nitrogen atmosphere at cryogenic temperatures. Upon completion of the test, the tubes were installed into the arrays (see Fig. 5) in the cleanroom at MPIK. After installation and also after transportation to LNGS, all tubes were tested successfully. The detector was filled with liquid xenon in April 2016 and since then, the photosensors are operating. First calibration data shows among others an improvement of a factor two in light yield compared to XENON100 which results in an improved energy threshold allowing for better sensitivity at low WIMP masses.

XENONnT and R&D Activities

In parallel to the ongoing data taking, the collaboration prepares for a quick upgrade of XENON1T. The so-called XENONnT experiment can re-use many critical hardware components of XENON1T and will have a total xenon mass of 7 tons [8] with a fiducial mass of around 3 tons. At the end of XENON1T the cryostat will be opened and only the cryostat's inner vessel as well as the XENON1T TPC will be removed and replaced by a

Fig. 6: The new automated emanation system (Auto-Ema). The piping and instrumentation is in front of the clean box containing the sample vessels.

larger inner vessel and the XENONnT TPC. A significant fraction of the necessary funds for XENONnT were already secured and procurement of the required xenon has already started. The design of XENONnT has started and will be continued and finalised in the next year when also the construction of components will start. The current schedule foresees the installation in the underground laboratory end of 2018. Consequently, the commissioning of XENONnT will start beginning of 2019 and at an exposure of 20 ton-years it will reach a sensitivity of 1.6×10^{-48} cm^2 for the spin-independent WIMP-nucleon cross section at a WIMP mass of 50 GeV/c^2 (Fig. 4).

Such an ambitious goal may only be achieved by further optimisation of the detector performance. As in XENON1T, the MPIK will be involved in the procurement of photomultiplier tubes (PMTs) and in the cleanliness of the detector with respect to both, radioactive and chemical impurities. XENONnT will re-use the XENON1T PMTs and needs around 230 new ones of which about 60 will be bought by MPIK. In cooperation with Hamamatsu the R11410 PMT will be further optimised with respect to light emission, tightness and stability.

In XENONnT, the selection of radiopure construction materials will become even more important than before. To enhance throughput and sensitivity we developed the GIOVE spectrometer (see Chapter 1.4, p. 39) with world record sensitivity at shallow depths due to a highly optimised shield as well as a new automated emanation setup (Auto-Ema) for ^{222}Rn screening (see Fig. 6). The time-consuming procedures for sample preparation and extraction of radon from the samples can now be performed in the most efficient way as the machine runs autonomous. Another benefit of Auto-Ema is that the individual measurements have a higher reproducibility which in turn reduces the systematic uncertainty and improves the detection limit. In the future Auto-Ema will not only be used for material screening, but also to investigate other possibilities for radon mitigation. A promising technique is surface coating. In principle a thin, tight and clean coating should be sufficient to block generated radon and delay its emanation until it decays. First tests with ^{220}Rn already showed promising results.

Another strategy in order to mitigate the ^{222}Rn-induced background is the permanent purification of the LXe target from the emanated radon before it disintegrates. We have investigated the development of such a radon removal system based on cryogenic distillation. Dedicated measurements show, that the ^{222}Rn concentration in boil-off xenon is reduced by a factor R>4 with respect to the liquid phase. This reduction power can be enhanced using a multiple-stage distillation column. During a radon distillation campaign at the XENON100 detector, we could demonstrate for the first time the ^{222}Rn reduction in a liquid xenon based experiment by a factor of D=20 by means of an online operated radon removal system. Further R&D projects are currently investigating its applicability in the XENONnT experiment.

Teresa Marrodan, Hardy Simgen, Manfred Lindner

Indirect Dark Matter Detection in TeV Gamma Rays

Indirect detection methods for dark matter rely on the annihilation of two dark matter particles into ordinary hadrons or leptons, resulting in final states containing particles, gamma rays and neutrinos. The flux of secondary particles is governed by an astrophysical factor – the line-of-sight integrated squared dark matter density – and a particle physics factor – the velocity-weighted annihilation cross section times the spectrum of final-state particles created per annihilation. Since the annihilation rate grows with the square of the density of dark matter, indirect detection techniques concentrate on regions with high dark matter density; most promising is the Galactic Centre region, but also nearby dwarf

galaxies. An estimate of the annihilation cross section can be obtained considering the balance between dark matter annihilation and dilution of dark matter density due to the rapid expansion in the early Universe: for (velocity-weighted) cross sections around $<\sigma v> \sim 3 \times 10^{-26}$ cm^3/s the right amount of dark matter is left over at the time when expansion effectively stops the annihilation. Since dark matter particles in galactic halos move at velocities low compared to the speed of light, the annihilation proceeds effectively at rest and the spectrum of secondary particles cuts off at the rest mass of the annihilating particles, providing a characteristic signature. Specific annihilation modes provide line-like signatures at or near this kinematic limit.

Data from 10 years of H.E.S.S. observations of the Galactic Centre region has been analysed searching for signs of annihilating dark matter, based on a total of 254 h of data [11]. In order to minimise contamination from astrophysical emission along the Galactic Plane (see Chapter 1.2), a band of ±0.3° in Galactic latitude is excluded; outside this region, the possible contribution of annihilation gamma rays is determined from a likelihood fit making use of the predicted distribution of annihilation gamma rays in space and energy, for a given annihilation channel and dark matter distribution, using regions at larger distance from the Galactic Centre for background estimates. No indication for dark matter annihilation is found, but for the first time, the resulting limits on the velocity-weighted annihilation cross section in the TeV mass range reach the predicted thermal annihilation cross section for certain modes (Fig. 7), providing a real test of models.

A search for dark matter line-like signals was performed in the vicinity of the Galactic Centre by the H.E.S.S. experiment on observational data taken in 2014, including data from the new H.E.S.S. II telescope and expanding the energy range to lower energies, providing overlap with results from the space-based Fermi gamma-ray observatory (Fig. 8). No significant excess associated with dark matter annihilations is seen in the energy range 100 GeV to 2 TeV, in particular ruling out at 95% C.L. the presence of a 130 GeV line previously reported in Fermi-LAT data. These current H.E.S.S. results define the state of the art of indirect dark matter detection in the TeV domain. CTA (see Chapter 1.1) will be nearly 10 times more sensitive than H.E.S.S. and will be able to detect dark matter in the TeV range, or exclude a significant region of the parameter space.

Jim Hinton, Werner Hofmann, Aion Viana

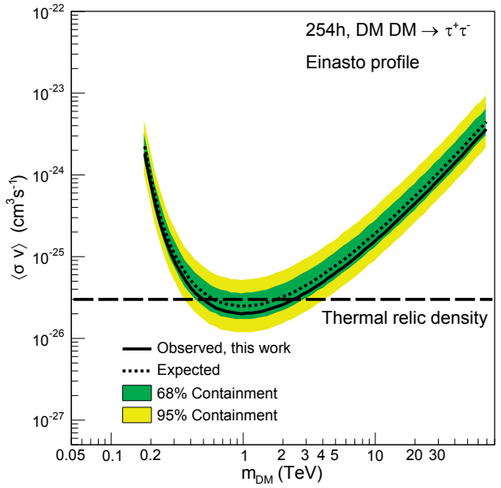

Fig. 7: Constraints on the velocity-weighted dark matter annihilation cross section <σv> for the τ⁺τ⁻ channels derived from observations taken over 10 years of the inner 300 pc of the GC region with H.E.S.S.

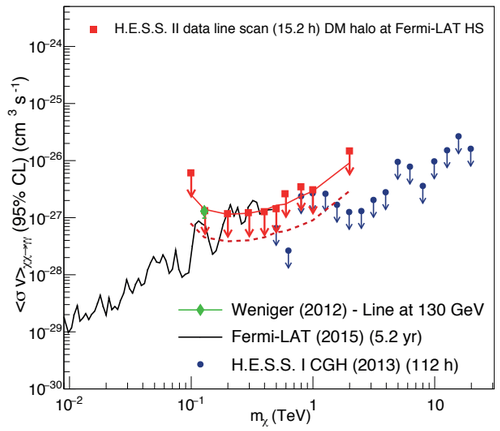

Fig. 8: <σv> limits for the line scan between 100 GeV and 2 TeV, based on H.E.S.S. II data.

References:

[1] F.S. Queiroz et al., J. Cosmol. Astropart. Phys. 1605 no.05, 050 (2016)
[2] W. Rodejohann et al, J. Cosmol. Astropart. Phys. 1512 no.12, 032 (2015)
[3] P. Grothaus, M. Lindner, Y. Takanishi, J. High Energy Phys. 1307, 094 (2013)
[4] F.S. Queiroz et al, arXiv: 1610.06581
[5] M.D. Campos et al, Phys.Rev. D94 no.9, 095010 (2016)
[6] XENON100, Science 349 851 (2015)
[7] XENON100, (2016) arXiv:1609.06154
[8] XENON1T, J. Cosmol. Astropart. Phys. 04, 027 (2016)
[9] S. Lindemann, H. Simgen, Eur. Phys. J. C 74, 2746 (2014)
[10] XENON1T, Eur. Phys. J. C75 no.11, 546 (2015)
[11] H.E.S.S. Collaboration, H. Abdallah et al., Phys. Rev. Lett. 117, 111301 (2016)
[12] H.E.S.S. Collaboration, H. Abdallah et al., Phys. Rev. Lett. (in press), arXiv:1609.08091

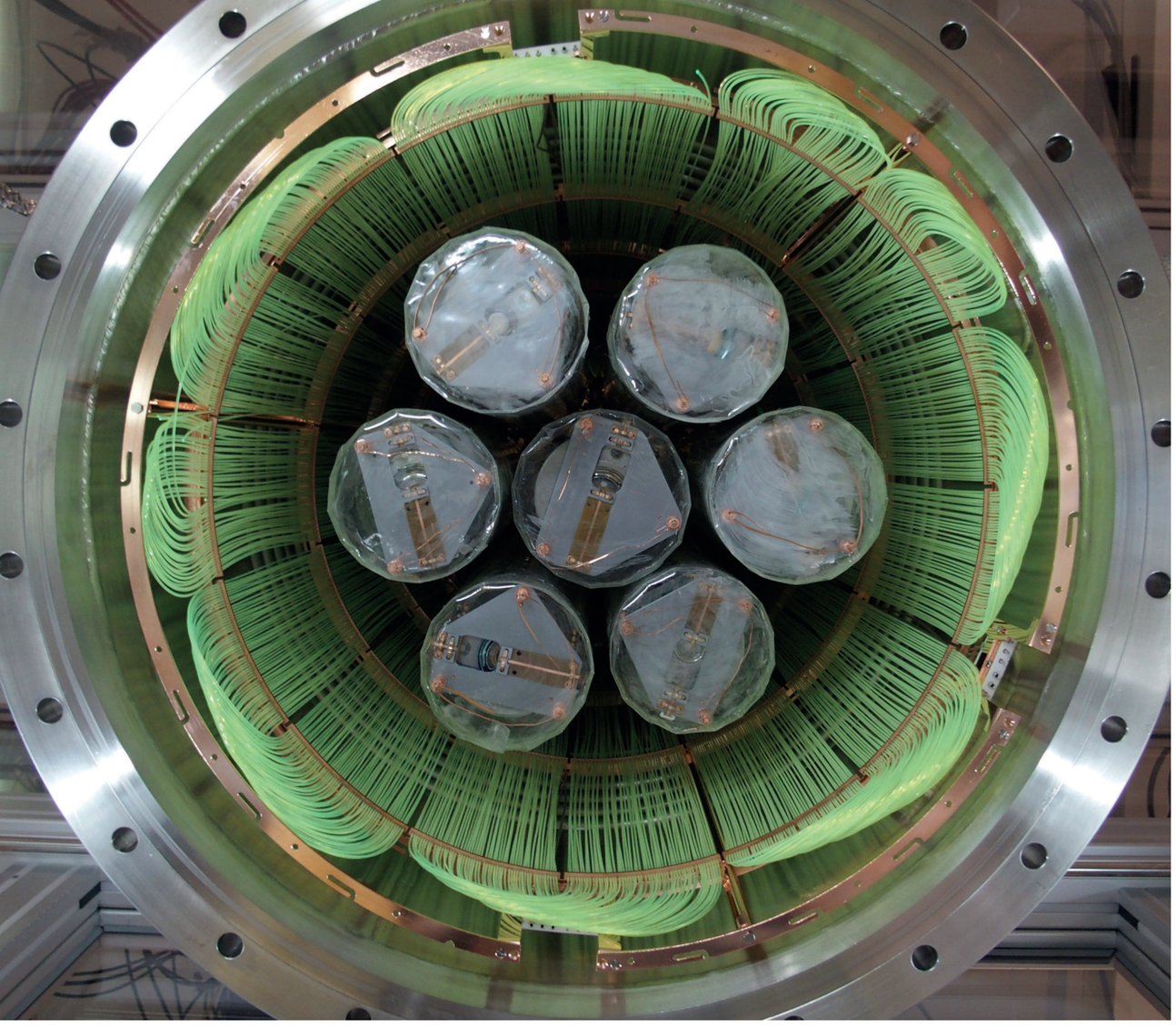

Bottom view on the seven strings of germanium detectors in Phase II of GERDA. The detectors are placed in nylon cylinders. The green scintillating fibres are part of the liquid argon veto system.

1.4 Neutrinos

Introduction

Neutrino mass remains the only physics beyond the Standard Model (SM) testable in the lab. It is expected to provide valuable hints towards the theory that lies behind the SM. In order to analyse the implications of neutrino physics, one needs to determine the measurable parameters with high precision, look for deviations from the standard picture, and theoretically interpret the experimental results from a broader perspective.

Neutrino Theory

Interpreting the experimental neutrino results, one has to face the main challenges: What is the mechanism behind neutrino mass? Is there a pattern behind the structure of lepton mixing? What do the measured neutrino parameters imply for the unknown ones? How can one apply the neutrino oscillation mechanism in extreme conditions? Is the standard paradigm of three massive Majorana neutrinos correct?

The simple textbook formalism of neutrino oscillations faces problems when extreme conditions are met, such as extremely high densities during certain phases of supernova explosions. Dense neutrino backgrounds lead to complex collective phenomena, such as synchronised oscillations, bipolar oscillations and spectral splits and swaps. Delicate quantum mechanical complications arise as a consequence, and a proper understanding is important to extract information about neutrino physics and the explosion mechanism, once a galactic supernova is observed. This, in particular issues of loss of coherence, has been studied [1]. In addition, the application of the Liouville equation for describing supernova neutrino oscillations was investigated.

The emerging structure of lepton mixing with large and close-to-maximal mixing angles indicates the presence of an underlying flavour symmetry, see Fig. 1. Residual symmetries are often crucial. This means that the flavour symmetry is broken in such a way that certain subgroups remain conserved in the neutrino and/or charged lepton sector, and eventually fully determine the observed mixing pattern. By properly breaking the flavour symmetries, one can therefore generate certain mixing schemes, such as symmetric mixing matrices, or patterns with maximal mixing and phases [2].

Incorporating the flavour symmetry in larger symmetries such as left-right symmetric or grand unified theories, is very challenging since the constraints that are imposed in such theories (e. g. connected Yukawa coupling matrices for different particle species) make it very difficult to construct successful theories. General aspects of residual symmetries in grand unified theories were studied and flavour symmetry models within left-right symmetric theories constructed.

Aspects related to the phenomenology of lepton mixing are analyses on the robustness of model predictions, of properties of unitarity triangles, and of neutrino flavour ratios of astrophysical neutrinos as studied in IceCube.

The question of Majorana neutrinos and neutrinoless double beta decay, or lepton number violation in general, was analysed with various approaches. In case the decay is mediated by light massive Majorana neutrinos, the so-called effective mass determines its lifetime. The fact that the effective mass is nonzero in the inverted mass ordering allows

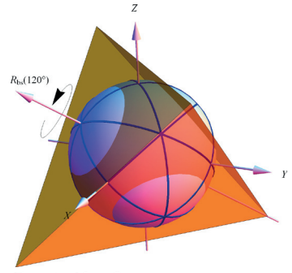

Fig. 1: If a flavor symmetry corresponds to the symmetry of the tetrahedron, rotations by 120 and reflections by 180 degrees are part of the symmetry, i.e. related to subgroups. The 180 degree reflections are chosen here as x-, y- and z-axes; the 120 degree rotation can be chosen such that it bisects a plane built by two axes. It can be shown that the group can be broken such that the resulting mixing matrix is symmetric. From [2].

to rule out this ordering if neutrinos are Majorana particles, or even show that neutrinos are Dirac particles in case an inverted ordering is determined by oscillation experiments. In this respect, the importance of precision determination of lepton mixing angles was studied. The future JUNO reactor neutrino experiment will determine the solar neutrino mixing angle with negligible uncertainty. This fixes the lower value of the effective mass in the inverted ordering and reduces the range of half-life predictions in order to test this value by a factor of two. The remaining uncertainty is caused by nuclear matrix elements.

Another aspect investigated was that if the effective mass is around zero, one still can deduce interesting information on neutrino parameters, assuming that neutrinos are Majorana particles.

Many alternative mechanisms for neutrinoless double beta decay exist, in particular within left-right symmetric theories. In those cases the decay is mediated by heavy TeV-scale particles, implying collider physics tests of the mechanism. In these cases predictions on the lifetime are decoupled from strong cosmological neutrino mass limits, and also from the determination of the neutrino mass ordering in oscillation experiments.

Models that generate neutrino masses and lepton mixing induce new particles, which often couple to the Higgs boson. Several consequences can arise now: (i) nonstandard Higgs decays, either modified decay rates into SM particles or decays into new particles; (ii) modification of the stability of the electroweak vacuum, which is determined by the running of the quartic Higgs self-coupling; (iii) naturalness issues, caused by corrections to the Higgs mass from loop-corrections involving the new particles responsible for neutrino masses.

Regarding the vacuum stability, the type I seesaw mechanism involving right-handed neutrinos is particularly relevant. If the Higgs quartic coupling becomes negative at some energy scale, our electroweak vacuum is not the true minimum and decay into the true minimum can occur. Thermal fluctuations at high temperature in the early Universe can also lead to transitions in the true vacuum. In the pure Standard Model case the coupling indeed becomes negative at scales of about 10^{11} GeV, but the resulting lifetime of the vacuum is much larger than the age of the Universe, hence the electroweak vacuum is metastable. In many mechanisms for neutrino mass, in particular the type I seesaw, this may change. This is because the Yukawa coupling Y_ν of the neutrinos to the Higgs and lepton doublets contributes to the running of the quartic coupling in such a way that it becomes earlier and more negative [3], see Fig. 2.

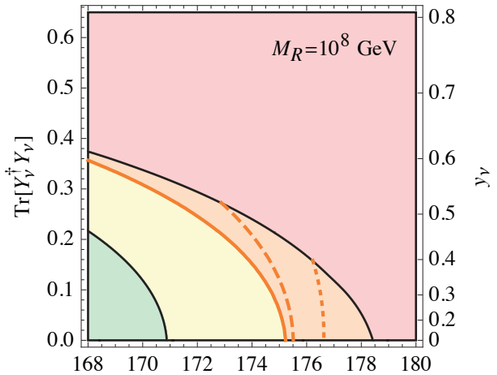

Fig. 2: Constraints on the neutrino Yukawa coupling Y_ν and the top quark mass. The plane is divided into regions of absolute stability (green), zero temperature quantum mechanical tunneling metastability (yellow and orange), and instability (red). The orange region corresponds to an instability due to thermal transitions in the early Universe, assuming a maximum temperature achieved in the Universe of $T_{max} = 10^{18}$ GeV. The region shrinks according to the dashed and dotted orange lines for lower maximum temperatures of 10^{15} GeV and 10^{12} GeV, respectively [3].

Neutrinos are produced as final states of beta decays. In this respect, the upcoming KATRIN experiment is actively pursuing R&D towards modifying the experiment in order to test the full electron energy spectrum, i.e. not only the region close to the endpoint. This opens up the possibility to probe neutrino masses up to tritium's Q-value of 18.6 keV, touching the region where such neutrinos are warm dark matter candidates. Also exotic charged current interactions are testable. Consequences for left-right symmetric theories and of frameworks with extra dimensions were analysed. Performing for a general set of interactions (scalar, tensor, etc.) a fully relativistic calculation, the distortions of the spectrum were calculated. Improving the current limits on the exotic interactions by more than 2 orders of magnitude is possible [4].

Various possibilities for nonstandard neutrino physics exist. Those include e.g. nonstandard interactions, which denote here flavour non-diagonal neutral current terms, mediated possibly by new TeV-scale physics. It was demonstrated how such interactions can modify the determination of the standard CP phase in future long baseline experiments. Another example in which new physics spoils the extraction of standard physics parameters is if the low energy PMNS matrix is non-unitary.

Since almost two decades hints exist (most notably the LSND experiment and the reactor anomaly) which point to the existence of sterile neutrinos, i.e. Standard Model fermion singlets with mass of order eV, weakly mixing (with ~10%) with the active neutrinos. In order to suppress their potentially strong consequences in cosmology (their contribution to the sum of neutrino masses and to the number of effective degrees of freedom) one can introduce new gauge interactions for the sterile neutrinos. Explicit models were constructed, and current constraints on such models from laboratory measurements were obtained.

A new window to study mixing parameters of sterile neutrinos was opened by the IceCube experiment. High-energy atmospheric neutrinos are sensitive to sterile neutrinos due to their influence on the survival probability of muon neutrinos. Particular emphasis needs to be put on the question whether such an analysis can rule out sterile neutrino hints. While important complementary information is provided, the different dependence on the various sterile neutrino mixing angles makes it currently not possible to fully exclude short baseline appearance results or sterile neutrinos in general.

Manfred Lindner, Werner Rodejohann

Double Chooz: Reactor Neutrino Oscillations

Nuclear reactors are a strong and pure source of electron antineutrinos well suited to study neutrino properties, and this allows Double Chooz (DC) to determine the neutrino mixing angle θ_{13}. The basic concept is a near and a far detector of identical design providing a clean measurement of this neutrino mixing angle without relying on the flux normalisation by simulations. The near detector at a distance of ~400 m to the reactors monitors the neutrino rate since 2015 at a position where the oscillation effect is small. Since 2011, the far detector detects the disappearance of the electron antineutrinos at 1.05 km distance.

The neutrinos are detected in an inverse beta decay reaction on protons in an organic liquid scintillator (target). The interaction signature of neutrinos with energies above the reaction threshold of 1.8 MeV is a coincidence signal of a prompt positron and a delayed neutron capture. The target is doped with 1 g/l of Gd for more efficient neutron capture. The liquid scintillators (LS) in DC were developed, produced and characterised at MPIK. The detector response (<1% variation per year) and neutron capture efficiency (<0.2% variation per year) were found to be stable for more than 5 years now. The target liquid with a mass of 8.3 tons is surrounded by about 18 tons of Gd-free LS called gamma catcher (GC) both contained in cylindrical acrylic vessels. The liquids of the inner detectors are completed by 80 tons of non-scintillating buffer oil, contained in a steel vessel with 390 photomultiplier tubes (PMTs) of 10 inch diameter, another MPIK hardware contribution (see Fig. 3). Two systems are available for muon detection. There is an inner veto (IV) consisting of 70 tons of LS and an outer veto (OV) made out of flat layers of plastic scintillator strips on top of the detector. MPIK also contributed to the deployment of radioactive gamma sources and a Cf neutron source along the target centre for calibration purposes.

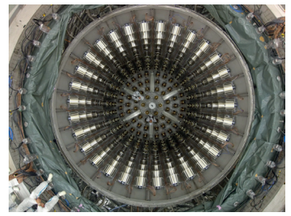

Fig. 3: Top view of the open Double Chooz near detector.

In the Gd analysis of DC we look for the coincidence signal after a muon veto of a prompt positron candidate (0.5-20 MeV) and a high-energy (4-10 MeV) delayed event after neutron capture by Gd within a coincidence time window of 0.5-150 µs. With additional optimised selection cuts the signal to background ratio in DC could be increased to more than 25. The small contribution of accidental background from random coincidences can be measured with high precision. However, if neutron captures by hydrogen are included in the analysis, this type of background increases due to the lower delayed energy of 2.2 MeV. Therefore, a multivariate analysis based on an artificial neural network was implemented for accidental background reduction. Correlated signals of fast spallation neutrons are partially tagged by the IV and can be measured at higher energies above 10 MeV where this type of background dominates the event rates. Correlated background from untagged muons decaying inside the detector is largely suppressed using information from the vertex reconstruction. Finally, there is background from long-lived cosmogenically produced β-n emitters like ^{9}Li or ^{8}He. A dedicated veto allows to partially reject β-n events. The remaining β-n background rate is best determined in the rate plus shape oscillation fit directly. Additionally, measuring the background in reactor-off periods (about 7 days so far) can be used to further constrain the total background rate in the neutrino oscillation analyses.

The first DC analyses were based on a fit including rate and shape information using only events with neutron captures by Gd. Then a rate-only analysis fitting the observed anti-neutrino rates for different reactor power conditions was developed [5, 6]. The result of this approach is independent of any background model and yields a simultaneous measurement of the two fit parameters θ_{13} and total background rate. A disjoint and larger sample of events was obtained by searching for neutrino candidates with neutrons captured by H [7]. In this way the fiducial volume could be extended to the GC liquid. All methods provided consistent results. In the first years of DC, θ_{13} was determined with data from the far detector only. After two years of data taking with two detectors we obtained $\sin^2(2\theta_{13}) = 0.119 \pm 0.016$ (see

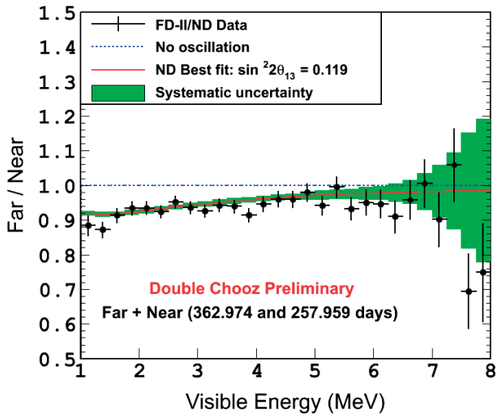

Fig. 4: Ratio of measured far detector to near detector rate. The oscillation effect is clearly visible at low energies.

Fig. 4), about 2σ above the best fit values of Daya Bay and RENO. To improve the statistical power of DC, neutron captures by H were included in the neutrino selection increasing the neutrino rate in the near (far) detector to about 900 (140) per day. MPIK provided large contributions to the DC analysis, in particular the determination of the neutron detection efficiency for the delayed neutrino signal and energy scale studies. Related systematic uncertainties were investigated using calibration data and MC simulations.

During the analysis structures in the prompt neutrino spectrum were found which are not expected from shape calculations [1]. It could be shown that an excess of events as compared to predictions from the reactor power and fuel composition around 5 MeV is correlated with the reactor flux which disfavours explanations based on unknown background contributions. The feature is observed in both detectors for the Gd and H data samples independently and it is also detected in other experiments. Our new data with the near detector will allow more detailed studies of the neutrino spectrum and might help to find the explanation of this anomalous shape behaviour.

Christian Buck, Julia Haser, Stefan Schoppmann

Nucifer: Applied Reactor Neutrino Physics

The radioactive decays of fission products in nuclear reactors produce isotropically emitted electron antineutrinos. The antineutrino spectrum and yield is not the same for the different fission isotopes ^{235}U, ^{238}U, ^{239}Pu and ^{241}Pu. Therefore, a measurement of the antineutrino flux close to nuclear reactors allows characterising the conditions of the reactor interior like fuel composition and thermal power. The Nucifer experiment [8] investigated whether neutrino detectors could be used for safeguard or nonproliferation applications. The Nucifer detector was placed at a distance of only 7.2 m from the Osiris research reactor (70 MW) at CEA Saclay in France. The detector target consists of 850 litres of a Gd-loaded liquid scintillator developed at MPIK. The neutrinos are detected via inverse beta decay on hydrogen atoms in the target scintillator. It could be shown that the presence of about 1.5 kg ^{239}Pu in an Osiris-like reactor could be detected at 95% C.L. This is of interest with regard to the Plutonium Management and Disposition Agreement for the disposal of weapon-grade Pu. The demonstrated stability allows for a relative monitoring of the neutrino rate within a few percent over several years with little maintenance. Therefore, Nucifer meets basic requirements of a suitable IAEA monitoring apparatus at nuclear reactors.

Nucifer can also be used to learn more about the reactor neutrino anomaly. The neutrino flux measured in many experiments close to nuclear reactors (~100 m) is significantly about 6% lower than the predicted flux rate. This effect, known as reactor neutrino anomaly, could be explained by oscillations of active into sterile neutrinos, which are not detected by the experiments. Other possibilities such as additional uncertainties in the theoretical flux calculations are also considered. In Nucifer the mean number of detected antineutrinos is $281 \pm 7\,(\text{stat}) \pm 18\,(\text{syst})$/day. This value is in agreement with no-sterile neutrino predictions (277 ± 23/day), but due to the large systematic uncertainties in Nucifer not conclusive in terms of the light sterile neutrino search.

Christian Buck

Stereo: The Search for Sterile Neutrinos

The Nucifer experiment is rather limited in sensitivity for sterile neutrino searches, mainly due to its high background and the missing segmentation. Other experiments more optimised for sterile neutrino search are currently under construction or just started operation. One of them is the Stereo experiment at the Institut Laue-Langevin (ILL) in Grenoble, France. The Stereo detector is positioned about 10 m away from a 58 MW research reactor highly enriched with ^{235}U. The 2.2 m long detector has a neutrino target

segmented in six identical cells, all of them filled with an organic liquid scintillator (LS) doped with a Gd complex. The pattern arising from active to sterile neutrino oscillations depends both on the neutrino energy and the distance from the core to the detection vertex. The six target cells at different distances from the reactor core aim to measure the relative distortions of the neutrino energy spectrum.

The reactor antineutrinos are observed by their interaction with the organic scintillator H nuclei. In the Inverse Beta Decay (IBD) reaction a correlated signal from the emitted positron and neutron is detected. The more than 1800 litres of neutrino target are surrounded by another 2100 litres of Gd-free liquid scintillator to detect escaping gammas. The produced scintillation light is collected by a set of 48 photomultiplier tubes (PMTs). As a consequence of the reactor vicinity and the surrounding neutron beam lines, the Stereo environment has a high background level of neutrons and gammas. For that reason a heavy shielding made of B_4C, lead and borated polyethylene surrounds the detector. In addition, a water Cherenkov veto is placed above the detector to tag cosmic muons at the shallow depth of the site. Stereo is expected to measure 400 neutrinos per day, and after a period of 2 years it will be able to probe the main part of the allowed parameter region of the reactor antineutrino anomaly (see Fig. 5). The detector was filled in November 2016 and data taking has started.

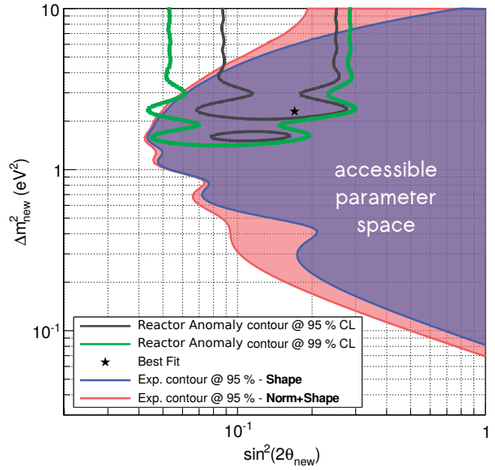

Fig. 5: Stereo sensitivity to sterile neutrino parameters.

The MPIK made crucial contributions to the central part of the detector as the PMTs and inner detector liquids. All PMTs were carefully characterised prior to their installation inside our light-tight 30 m^3 Faraday chamber. As a light source to perform the characterisation tests, LED boards developed by the electronics workshop at MPIK were configured to produce light at an adequate wavelength with tunable intensity. Additional PMT mechanics and structure to hold them inside the detector were fabricated in our workshop. For the liquid scintillator chemistry we benefit from our Double Chooz and Nucifer experience and related infrastructure. The Gd-beta-diketonate complex, which is dissolved in the target scintillator was purified by sublimation at Sensient company. Purification of the solvents was performed in our scintillator hall using columns packed with Al_2O_3. As compared to the solvents used in Double Chooz, the n-dodecane was replaced by LAB (linear alkyl benzene) to gain in light yield. The PXE (phenyl xylyl ethane) was kept at a concentration of about 20 wt.%, since it improves the light yield as compared to pure LAB as well as the pulse shape discrimination (PSD) capabilities for more efficient background suppression. It was found that adding diisopropyl naphtalene at 5% further improves the PSD. The final mixture should fulfil the requirements of material compatibility, mainly with the acrylic material inside the detector, suitable optical properties and long-term stability over several years of data taking. The detector was filled and is kept under nitrogen using systems designed at MPIK. Next, we also plan to contribute strongly to the upcoming data analysis.

A comparison of the neutrino spectrum measured in Chooz and Stereo might allow gaining new insights into the origin of the measured anomalous neutrino spectral shape. The Stereo reactor is highly enriched in ^{235}U whereas there is less enrichment in Double Chooz. Therefore, the Chooz reactors have higher contributions from the fission of Pu isotopes and ^{238}U. With a high precision on the energy scale uncertainty in both experiments, it should be possible to test if the shape distortion is either solely or not at all related to the predicted ^{235}U spectrum [9].

Christian Buck, Julia Haser, Stefan Schoppmann, Manfred Lindner

Borexino: Hunting Neutrinos from the Sun and Other Sources

Borexino is a large organic-liquid scintillator detector used mainly for the detection of solar neutrinos, but also of (anti)neutrinos from other extraterrestrial, terrestrial and artificial sources. It is located at the Laboratori Nazionali del Gran Sasso, Italy. Due to the achievement of unprecedented low background levels of its scintillator, real-time spectroscopy of low-energy (anti)neutrinos in the sub-MeV region has become possible. In Phase I of the experiment (2007-2010), the collaboration measured neutrinos from several fusion reaction

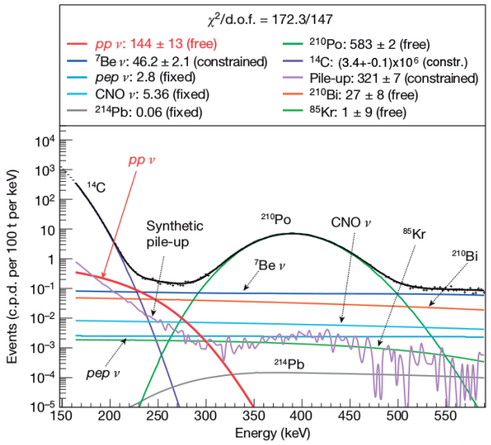

Fig. 6: Detection of solar pp neutrinos with Borexino: best fit of the energy spectrum in the range 165-590 keV.

processes in the Sun. In order to detect neutrino sources with even smaller count rates and lower energies, the residual radioactive contamination of the scintillator was further reduced by extensive purification campaigns in 2010-2011. Phase II, which is based on data collected after 2011 and is still on-going, has already led to several new results.

The collaboration succeeded to perform the first direct detection of the solar pp neutrinos (<0.42 MeV), which constitute 90% of the solar neutrino flux. The pp neutrino rate was determined to be $144 \pm 13\,(\text{stat}) \pm 10\,(\text{syst})$ counts per (100 ton · d) (see Fig. 6). The extrapolated flux is well in agreement with the Standard Solar Model (SSM) prediction and consistent with the most favoured neutrino oscillation scenario, in which resonant matter effects occur only for neutrinos with energies above few MeV by maximising the conversion of one flavour type to another one (so-called Large Mixing Angle solution including the Mikheyev-Smirnov-Wolfenstein effect). The pp measurement demonstrated that the correlated solar photon luminosity deduced from the SSM is in agreement with the photon luminosity obtained independently from photospheric measurements.

Borexino also published a new result about terrestrial antineutrinos. The used dataset covers the period from December 2007 to March 2015 and includes a total exposure of almost 1 kton · yr. Since the search for antineutrinos is based on a very distinct coincident signal from the antineutrino-induced inverse beta decay, it was possible to select a very clean sample of events: 77 antineutrino candidates were identified, of which less than 1 event is due to background. While $52.7 \pm {}^{8.5}_{7.7}\,(\text{stat}) \pm {}^{0.7}_{0.9}\,(\text{syst})$ events correspond to reactor neutrinos originating from European nuclear power plants, $23.7 \pm {}^{6.5}_{5.7}\,(\text{stat}) \pm {}^{0.9}_{0.6}\,(\text{syst})$ events are attributed to terrestrial antineutrinos. The latter result corresponds to a 5.9 σ discovery.

Beyond that, in the reporting period Borexino published new results about the search for other exotic rare processes such as Pauli forbidden transitions, solar axions and the non-conservation of electric charge, but also for extraterrestrial neutrinos from cosmic gamma-ray bursts. Among further challenging physics goals, Borexino is working towards the first direct detection of solar CNO neutrinos.

Werner Maneschg, Hardy Simgen

GERDA: Search for Neutrinoless Double Beta Decay

The dominance of matter over antimatter in our Universe cannot be explained by the Standard Model of particle physics. The favoured solution to this problem predicts that lepton number is not conserved and consequently a hypothetical process called neutrinoless double beta ($0\nu\beta\beta$) decay should exist. Its half-life would be at least fifteen orders of magnitude longer than the age of the universe, and – if observed – would be the rarest decay ever detected. The reduction of any background events mimicking the $0\nu\beta\beta$ decay is therefore of paramount importance for the experimental sensitivity.

The Germanium Detector Array (GERDA) located at the Gran Sasso underground laboratory in Italy searches for the $0\nu\beta\beta$ decay of ^{76}Ge according to $^{76}\text{Ge} \rightarrow {}^{76}\text{Se} + 2e^-$ by deploying germanium detectors in a liquid argon (LAr) bath. Source and detector for the decay are identical which results in a high detection efficiency. Also, the detectors are made from material isotopically enriched in ^{76}Ge to about 86%. The signature of the $0\nu\beta\beta$ decay would be a very faint peak at the Q-value $Q_{\beta\beta}$ (at 2029 keV) of this process. The argon (64 m^3) is free of thorium and uranium contaminations and is a perfect shield against external radiation. The cryostat is placed inside a tank of pure water (590 m^3) to complete the shielding.

GERDA proceeds in two Phases: Phase I concluded successfully in May 2013 after 1.5 years of data taking [10]. Since then the experiment has been upgraded and resumed operation with Phase II starting in December 2015. Since the Phase II upgrade the array is surrounded by a retractable 'LAr veto' system: a set of light detectors, SiPMs and photomultiplier tubes that are designed to detect argon scintillation around the germanium detectors and hereby efficiently suppress background events [11]. Also, the detector mass

has doubled by deploying several new germanium detectors, amounting to a total of 30 so-called BEGe-type detectors (20 kg) and seven coaxial-type detectors (15.8 kg) – for a view on the final setup see the title picture. For both detector types the time profile of detector signals is analysed to distinguish signal from background-like events: the combination of this pulse shape discrimination (PSD) with the LAr veto allows to expect less than one count in the region of interest around $Q_{\beta\beta}$ during Phase II, which means that GERDA will be the first "background free" experiment in the field.

First Phase II data collected until June 2016 and with an exposure of 10.8 kg · yr has been released. Again a blind analysis procedure is applied to avoid any human bias. Prior to unblinding the whole analysis chain, including the description of the background, quality cuts, and the PSD, has been frozen. The resulting energy spectra are shown in Fig. 7: for the Phase I dataset including an additional yet unpublished coaxial detector period from 2013 (top), and for the two Phase II datasets for the different detector types (middle and bottom). In case of the coaxial dataset, a total of four events survive all cuts at a PSD signal efficiency of $(79 \pm 5)\%$, which corresponds to a background index of $(3.5 \pm {}^{2.1}_{1.5}) \times 10^{-3}$ cts/(kg · keV · yr). Owing to an enhanced PSD performance, only a single event remains in the BEGe data set at a PSD efficiency of $(87 \pm 2)\%$ [12], resulting in a background level of $(0.7 \pm {}^{1.1}_{0.5}) \times 10^{-3}$ cts/(kg · keV · yr). Hence, the ambitious design goal of ~10^{-3} cts/(kg · keV · yr) has been met. GERDA finds no indication for a $0\nu\beta\beta$ decay of ^{76}Ge and settles a new, ever more stringent lower limit on the half-life $T^{0\nu}_{1/2} \geq 5.3 \times 10^{25}$ yr (90% C.L.) including systematic uncertainties. Assuming no signal, the (median) sensitivity on the lower limit yields 4.0×10^{25} yr.

For the Phase II upgrade, MPIK contributed large parts of the LAr veto, the novel detector holders, and the nylon cylinders surrounding the germanium detectors. We had a leading role during the characterisation of the detectors. Parts of the LAr veto analysis as well as the PSD analysis for all detectors have been done at the institute.

GERDA has successfully started the operation of Phase II with all detector channels working, and the background around $Q_{\beta\beta}$ is the lowest in the field. This is a major achievement. So far we have no hint for a $0\nu\beta\beta$ decay of ^{76}Ge, but GERDA Phase II will continue data taking for approximately two more years, and is ready to explore half-lives $\geq 10^{26}$ yr.

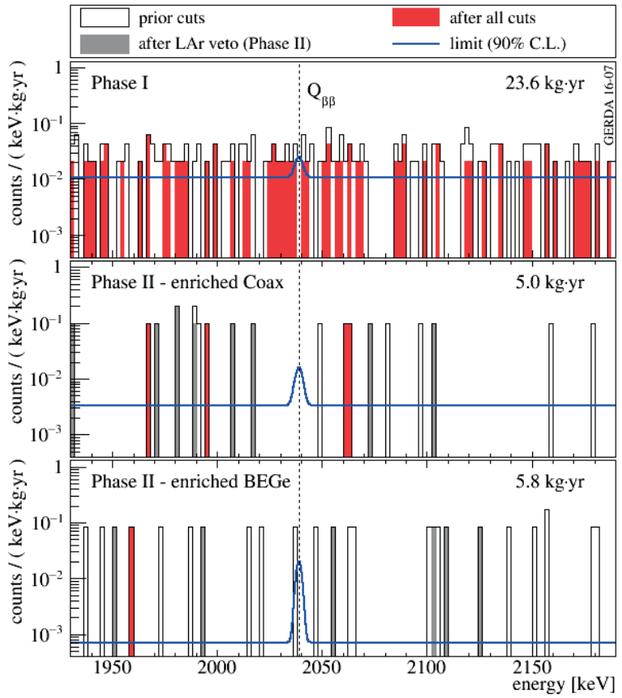

Fig. 7: Spectra for combined Phase I data (top), Phase II coaxial (middle) and BEGe detector data (bottom). The red histogram shows the final spectrum after all cuts, other colors are explained in the legend. The blue line indicates a fit to a hypothetical signal of $T^{0\nu}_{1/2} \geq 5.3 \times 10^{25}$ yr (90% C.L.) at $Q_{\beta\beta}$ assuming a flat background distribution.

Mark Heisel, Andrea Kirsch, Bernhard Schwingenheuer, Victoria Wagner

Advancements in Germanium Gamma-ray Spectroscopy and the Search for the Coherent Neutrino Nucleus Scattering

Characterisation of cosmic background at shallow depth. The GIOVE (Germanium Inner Outer VEto) detector setup is a new low-background Germanium spectrometer for the selection of materials with low radioactive content, which is located at the shallow depth (15 m of water equivalent) underground laboratory of MPIK [13]. It is equipped with a double active muon veto with a total muon rejection efficiency >99% and passive shield layers to moderate and capture neutrons. With this setup an integral count rate is achieved comparable to low-background Ge detectors operated far deeper underground. The obtained "virtual depth" corresponds to an overburden of several 100 m of water equivalent.

In the last three years, GIOVE has not only been used for material selection measurements, but also for the characterisation and simulation of the background components

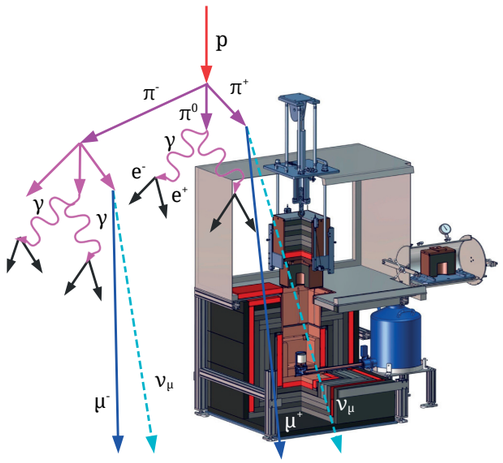

Fig. 8: Schematic drawing of the GIOVE spectrometer, which is crossed by a cosmogenic particle shower.

originating especially from the cosmic-ray muon-induced secondaries (see Fig. 8). These are subdivided into prompt electromagnetic showers and delayed de-excitation of metastable Ge isomeric states following e. g. captures of neutrons created by muons in the lead of the GIOVE shield. The simulated spectrum of the prompt muon-induced cascades turned out to be in excellent agreement (better than 10%) with the observed continuum and gamma lines [14]. However, concerning the expected number of neutrons at the diode, the simulation underestimates the measurement results by 40-80%. Dedicated studies including ^{252}Cf neutron source measurements confirmed these findings. The reason for the discrepancy has not yet been completely identified. Nonetheless, the semi-validated simulation has turned out to be a valuable tool to vary and optimise further the shield design of new Ge detectors at given depths, and to study the impact of new materials on the suppression of environmental and cosmogenic radiation.

Optimisation of germanium detector design. Over the last decade, several novel Germanium detector designs have emerged, which allow for lower noise levels as well as for improved energy resolutions and pulse shape discrimination capabilities compared to former designs. This has become increasingly attractive also for the search for neutrinoless double beta decay, for direct dark matter detection, searches for a neutrino magnetic moment, and for coherent neutrino nucleus scattering.

We investigated the possibility to further optimise the leading technology used in the current Phase II of the GERDA experiment, the so-called BEGe type. For this purpose two almost identical detectors of this type, each ~760 g, were acquired and the read-out electrodes stepwise modified according to specified simulations of the electric field in the detectors [15]. After each step, the detectors were extensively characterised under very similar measurement conditions. This unique study confirmed that the pulse shape discrimination efficiency of background signals at a few MeV can still be improved. Furthermore, the intrinsic noise of the detector can be reduced resulting in better energy resolution and lowered energy thresholds of 800 to 900 eV.

CONUS: Towards the detection of coherent neutrino nucleus scattering. Encouraged by the low background levels obtained with GIOVE and the low energy thresholds of the modified BEGe-type detectors, several feasibility studies were performed to observe still undetected physics phenomena at very low energies, for instance coherent neutrino nucleus scattering (CNNS). This process is one of six possibilities predicted by the Standard Model of Elementary Particle Physics, how neutrinos can interact with matter. A closer look at the process illustrates which challenges have to be met for an observation: (Anti)neutrinos of less than 50 MeV are expected to scatter coherently off a target nucleus, while the respective cross section should be enhanced by roughly the square of the number of neutrons in the nucleus. If an interaction takes place, the nucleus releases recoil energy, which – after a dissipation process known as quenching – is available for signal formation. Depending on the (anti)neutrino energy and the target nuclei, the available energy will be below few keV. Thus, three requirements have to be fulfilled for a CNNS detection: a high (anti)neutrino flux, an ultra-low energy threshold and a very low background in the region of interest. Former attempts to detect CNNS failed because of too high energy thresholds.

The newly established CONUS (COherent NeUtrino Nucleus Scattering) project aims at detecting CNNS signals by using germanium detectors and anti-neutrinos from a nuclear reactor as a source. Such reactor neutrinos have energies up to 8 MeV, resulting in a recoil energy of 2 keV for a Ge nucleus. Considering quenching effects, the maximum expected CNNS signal will have an energy of 400-500 eV.

The commercial nuclear power plant at Brokdorf has been selected for hosting the experiment. This reactor has a thermal power output of 3.9 GW making it one of the most powerful stations worldwide. The chosen experimental site is only at 17 m distance from the reactor core, allowing for an antineutrino flux of $2.5 \times 10^{13}/(s \cdot cm^2)$. The overburden thickness above the chosen place is roughly several tens of m of water equivalent.

A massive shield setup is being prepared at MPIK, which will accommodate up to four Ge detector cryostats. The overall dimensions of the CONUS shield design are smaller than

those of the GIOVE spectrometer, however it will also be equipped with an active muon veto and passive layers for neutron capture (s. Fig. 9). If the background levels achieved for GIOVE can be repeated for CONUS, the background index at energies below few keV is expected to match the desired level of 1 count/(day·keV·kg), with kg referring to the active mass of the Ge detectors. Each unit will house one 1-kg Ge diode, with a designed energy threshold better than 300 eV. This is below the expected maximum CNNS signal induced by reactor neutrinos scattering off Ge nuclei.

Altogether, the full CONUS setup is expected to detect several hundreds of events per year above the energy threshold, while yielding a good signal-to-background ratio. It is planned to install the shield and the Ge detectors at the Brokdorf nuclear power plant within 2017 and start data collection in the same year.

Janina Hakenmüller, Gerd Heusser, Werner Maneschg, Manfred Lindner

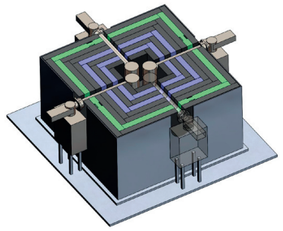

Fig. 9: Schematic drawing of the CONUS shield setup, in which up to four germanium detector cryostats can be embedded.

Silicon Photomultipliers: Light Readout for Low-Background Experiments

New concepts in ultra-low background experiments studying neutrino physics or searching for dark matter require advanced detector components, fulfilling ever stronger experimental requirements. The majority of these experiments involve detection of photons in the UV and visible wavelength range. Since fall 2015 we set forth in exploring the specifications of state-of-the-art SiPMs provided by leading manufacturers. A testing infrastructure has been set up, able to probe the majority of key features in a temperature range down to liquid nitrogen temperature. Custom-built preamplifiers were designed and produced at MPIK and their functionality proven down to temperatures of 100 K. We collected information about detector gain, charge resolution and contributions of spurious noise like afterpulses and crosstalk between pixels, see Fig. 10. Measurements of the breakthrough voltage V_{BR} and gain of the SiPM devices were performed and automatised, which allows studying other parameters as a function of the overvoltage (excess voltage with respect to V_{BR}). Next steps will encompass measurements of the high-resolution timing, coupling to light collectors and light guides to work towards the application in new neutrino and dark matter experiments.

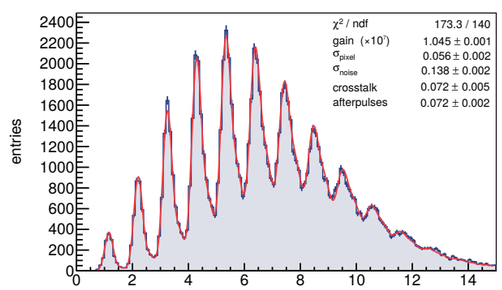

Fig. 10: Charge spectrum of multi-pixel events of a 3 × 3 mm² Hamamatsu SiPM at about –150 °C.

Julia Haser, Mark Heisel

References:

[1] E. Akhmedov, J. Kopp, M. Lindner, arXiv:1405.7275
[2] W. Rodejohann, X.J. Xu, Phys. Rev. D 91, 056004 (2015)
[3] M. Lindner, H.H. Patel, B. Radovcic, Phys. Rev. D 93, 073005 (2016)
[4] P.O. Ludl, W. Rodejohann, J. High Energy Phys. 06, 040 (2016)
[5] Y. Abe et al. (Double Chooz Collaboration), J. High Energy Phys. 10, 086 (2014) [Erratum ibid. 02 (2015) 074].
[6] Y. Abe et al. (Double Chooz Collaboration), Phys. Lett. B 735, 51–56 (2014)
[7] Y. Abe et al. (Double Chooz Collaboration), J. High Energy Phys. 01, 163 (2016)
[8] G. Boireau et al. (Nucifer Collaboration), Phys. Rev. D 93, 112006 (2016)
[9] C. Buck, A. Collin, J. Haser and M. Lindner, arXiv:1512.06656
[10] M. Agostini et al. (GERDA Collaboration), Phys. Rev. Lett. 111, 122503 (2013)
[11] A. Wegmann, PhD thesis, Universität Heidelberg (2016)
[12] V. Wagner, PhD thesis, Universität Heidelberg (2016)
[13] G. Heusser, M. Weber, J. Hakenmüller, et al., Eur. Phys. J. C 75, 531 (2015)
[14] J. Hakenmüller, W. Maneschg, G. Heusser, Proc. XIV Int. Conf. Topics Astropart. and Underground Phys. (TAUP 2015), J. Phys. Conf. Ser. 718, 042028 (2016)
[15] M. Salathe, PhD thesis, Universität Heidelberg (2015)

1.5 Particle Physics at Accelerators

View into the tunnel of the Large Hadron Collider (LHC) at CERN. The superconducting dipole magnets, operated at a temperature of 1.9 K, provide a guiding field up to 8 T for two counter-rotating beams. (Image: CERN)

Introduction

The Large Hadron Collider (LHC) at CERN, Geneva, currently is the world's most powerful particle accelerator, a storage ring with a circumference of 27 km, located at a depth of about 100 m under ground. It allows to accelerate and to collide protons and nuclei at nucleon-nucleon centre-of-mass energies up to 13 TeV, which corresponds to the rest mass of more the 13 000 hydrogen atoms. Since in high-energy collisions some of the kinetic energy of the collision partners is converted into matter and antimatter, these processes offer an ideal environment for the search of new particles and studies of differences between matter and antimatter.

Four large experiments study high-energy collisions at the LHC: two general purpose detectors (ATLAS and CMS), designed to search for new heavy particles and to study the Higgs boson, one experiment with focus on the study of heavy-ion collisions and the quark-gluon plasma that can be produced in such interactions (ALICE), and one detector optimised for precision measurements of matter-antimatter asymmetries and rare decays in the heavy flavour sector (LHCb).

A schematic view of the LHCb detector is shown in Fig. 1. It records particles emitted in inelastic collisions into the angular range between 15 and 300 mrad with respect to the beam. The momentum of charged particles is measured by a magnetic spectrometer, photons and neutral particles are detected using calorimeters. Cherenkov detectors and a muon system serve to identify the particles, and an elaborate filter system selects those events from the sample of all the interactions that contain information about the physics questions investigated with LHCb. From 2010 to the end of 2012, the experiment had collected a data sample corresponding to 2×10^{14} inelastic proton-proton collisions at centre-of-mass energies of 7 and 8 TeV. After a shutdown in 2013-2014, the LHC restarted at an energy of 13 TeV. Since spring 2015 the data sample recorded by LHCb has almost been doubled.

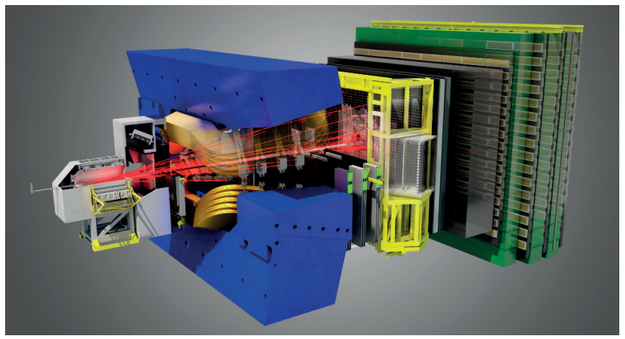

Fig. 1: Schematic view of the ca. 20 m long and 10 m high LHCb detector. The collision point is to the left of the spectrometer magnet (blue). Parts of the tracking system and the Cherenkov detectors are visible on both sides, to the right follow calorimeter and muon system.

The experiment is operated by an international collaboration of scientists from 69 institutes in 16 countries. The LHCb detector has about a million read-out channels, nearly half of which are equipped with silicon sensors. The MPIK has contributed the "Beetle" front-end chips for all of these components, the complete read-out electronics for half of them, and a sizable fraction of the sensors. The chips are an in-house development because commercially available devices would not withstand the radiation environment of the experiment. LHCb with its excellent tracking, vertexing and particle identification capabilities in a kinematic region not accessible to the other experiments, is not only making essential contributions to the field of heavy flavour physics, but also to electroweak and QCD studies. In the following a few physics highlights will be presented, where MPIK had a significant share in the results obtained by the LHCb experiment.

Flavour Physics

The large production cross-section for b and c quarks has made LHCb the dominant experiment in the field of flavour physics. Many measurements probe quantum corrections to the Standard Model and thus are susceptible to effects from new virtual particles, thereby looking for New Physics in a way complementary to, but with similar sensitivity as the direct searches by the general purpose detectors ATLAS and CMS. Of particular interest are rare decays, which are suppressed in the Standard Model and where even small (on an absolute scale) contributions from New Physics would have a large relative impact.

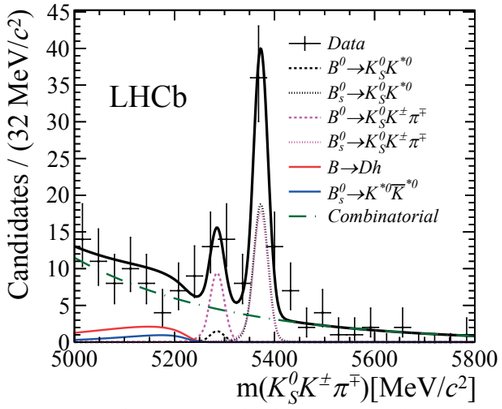

Fig. 2: First observation of the decay $B^0_s \to K^0_S K^{*0}$.

Fig. 2 shows the first observation of the decay of B_s mesons, bound states of a bottom and a strange quark, into two neutral kaons, K^0_S and K^{*0}. The K^0_S decays with an average lifetime of 0.1 ns into two oppositely charged pions, the other one is an excited state that immediately decays into a charged kaon and a charged pion. Only very little background is observed under the peak. The background is mainly combinatorial, i. e. contributions from other B-meson decay modes are negligible. The observed branching fraction [1] is $(10.9 \pm 2.8) \times 10^{-6}$, i. e. from about 100 000 initially produced B_s mesons, only one decays in this mode. At the current experimental precision the result is consistent with the Standard Model expectation.

Another process that has been studied is the decay of neutral D mesons into two K^0_S mesons, i. e. a rare decay of charm particles into a final state that is an eigenstate under the combined transformation of charge conjugation and parity. Different decay rates of D^0 mesons and their antiparticles, which can be identified through their production mechanism, into such a CP eigenstate would establish CP violation, a breaking of the symmetry between matter and antimatter, in the charm sector. Since the Standard Model predicts only very small CP asymmetries for charm particles, the measurement is sensitive to New Physics that may not be visible in the B-meson systems. Despite the large data volumes collected by LHCb, the analysis is extremely challenging since it requires to find, close to the point of the primary proton-proton interaction, a detached vertex from the two K^0_S mesons, which themselves are reconstructed through their decays that in LHCb typically occur tens of cm downstream from their point of origin. Using the data collected in 2011 and 2012, this decay mode is seen and a CP asymmetry $A_{CP} = -0.029 \pm 0.056$ is measured [2], which is more than three times more precise than the previous world best measurement.

Cross-Section Measurements

A fundamental quantity describing high-energy proton-proton collisions is the inelastic cross-section. Despite significant progress in the numerical solution of quantum chromodynamics, it is still not possible to calculate its value from first principles. Phenomenological models assume a rise with energy according to a power law within the Froissart-Martin bound, which asymptotically is proportional to the square of the logarithm of the centre-of-mass energy. Fig. 3 shows the result of a measurement of the inelastic proton-proton cross-section at a centre-of-mass energy of 7 TeV [3], compared to extrapolations from low-energy results. Within uncertainties measurement and extrapolation agree. The general trend is still well described by a power-law, i. e. the expected asymptotic behaviour is not yet seen at LHC energies.

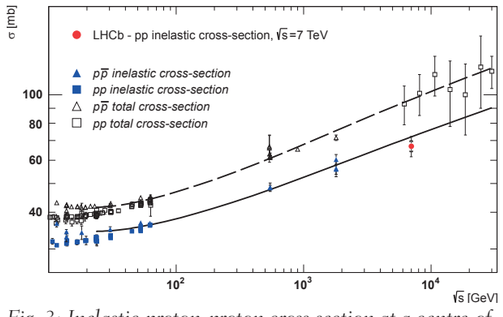

Fig. 3: Inelastic proton-proton cross-section at a centre-of-mass energy of 7 TeV, compared to extrapolations of results from lower energies.

Another measurement is the cross section for the production of Υ mesons [4] (bound systems of a bottom and an antibottom quark), which, as described below and also holds for bound states of a charm and anticharm quark, allow to probe the properties of a nuclear matter in high-energy hadronic interactions. Proton-proton collisions provide a baseline measurement, which can be compared to proton-lead and lead-lead collisions. In sufficiently central lead-lead collisions a quark-gluon plasma is expected to form, i. e. a high-temperature system of free quarks and gluons where bound quark-antiquark states are expected to melt as a consequence of Debye screening of the colour charges. Since the melting temperature is proportional to the binding energy, the relative suppression of the different Υ states allows to infer the temperature of the medium.

However, already the nuclear environment, with nuclear parton density functions (PDFs) that differ from those of the free protons, and where final-state particles created in the collision experience energy loss effects in the nuclear medium, can lead to a suppression in the production rates of Υ mesons. To explore the properties of a quark-gluon plasma, these cold nuclear matter effects, which can be studied in proton-lead collisions, need to be understood.

Data from proton-proton collisions with a centre-of-mass energy of 2.76 TeV are displayed in Fig. 4, showing clear signals for the Υ(1S) ground state and the first two excited states on an exponentially falling background. The centre-of-mass energy matches the nucleon-nucleon centre-of-mass energy of lead-lead collisions recorded earlier by the other LHC experiments. Combined with measurements at centre-of-mass energies of 7 and 8 TeV, it also allows to interpolate the reference cross section at intermediate energies, needed for the study of cold nuclear matter effects in proton-lead collisions [5].

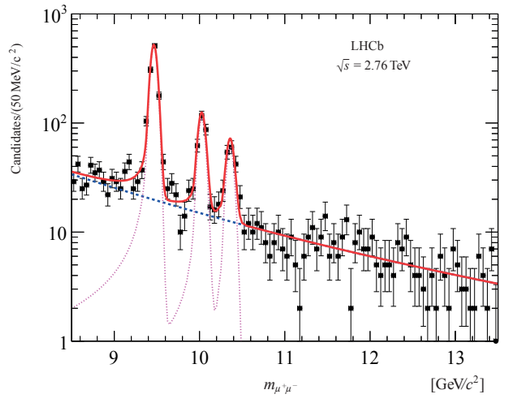

Fig. 4: Υ(1S), Υ(2S) and Υ(3S) production in p-p collisions.

Ion Physics and Fixed Target Interactions

Since 2012 the LHCb collaboration has expanded its physics programme to encompass also interactions involving heavy ions and fixed-target collisions. From the analysis of the proton-lead collisions recorded in February 2013, Fig. 5 shows the nuclear modification factor R_{pPb} (the production cross sections normalised to the number of nucleons per lead ion and the cross section in proton-proton collisions) for prompt J/ψ and ψ(2S) mesons (bound systems of a charm and an anticharm quark), as a function of the rapidity in the nucleon-nucleon centre-of-mass system [6].

The deviation from unity demonstrates the presence of cold nuclear matter effects. The J/ψ data are in good agreement with predictions based on leading-order nuclear PDFs. The agreement degrades at next-to-leading order, but is recovered if energy loss effects in the nuclear medium are accounted for. The data for ψ(2S) production show larger deviations from unity than for the J/ψ, which supports the picture that weaker bound systems are stronger affected by cold nuclear matter effects.

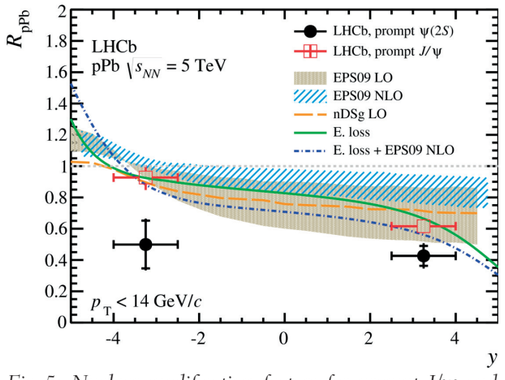

Fig. 5: Nuclear modification factors for prompt J/ψ and ψ(2S) production in p-Pb collisions as a function of rapidity. Positive rapidities are in the direction of the proton beam.

Since 2015, after the restart of the LHC, the LHCb experiment also participates in the lead-lead running and regularly takes fixed-target physics data with its so-called SMOG system, which allows to inject small amounts of noble gases (He, Ne, Ar) into the LHCb interaction region. With these data LHCb is able to look for quark-gluon plasma signatures in peripheral to semi-central lead-lead collisions, to study electromagnetic interactions at extreme field strengths, and for the first time to analyse in the lab interactions of multi-TeV particles on a fixed target, as they occur in the interactions of high-energy cosmic rays with the earth's atmosphere.

Michael Schmelling

References:

[1] LHCb Collaboration, J. High Energy Phys. 01, 012 (2016)
[2] LHCb Collaboration, J. High Energy Phys. 10, 055 (2015)
[3] LHCb Collaboration, J. High Energy Phys. 02, 129 (2015)
[4] LHCb Collaboration, Eur. Phys. J. C74, 2835 (2014)
[5] LHCb Collaboration, J. High Energy Phys. 07, 094 (2014)
[6] LHCb Collaboration, J. High Energy Phys. 03, 133 (2016)

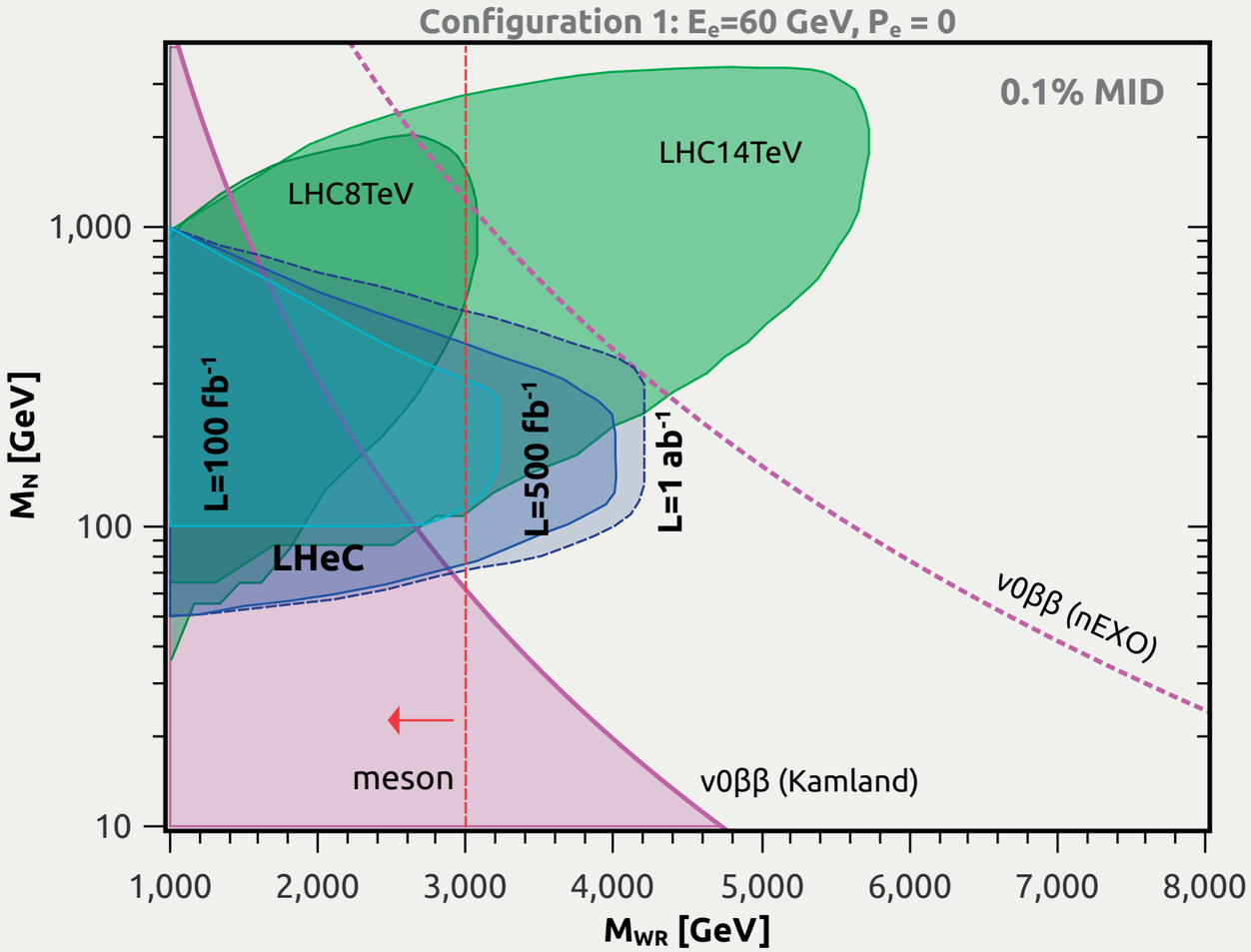

1.6 Physics beyond the Standard Model

Parameter space of right-handed neutrino and W_R mass as reachable by the LHC and the LHeC. The regions constrained by neutrinoless double beta decay experiments and meson oscillations are also shown. From [3].

Introduction

The Standard Model (SM) of particle physics is very successful in describing subatomic physics. A number of experimental and theoretical reasons are, however, known which strongly point to the fact that the SM is incomplete and that at some higher energy it must be embedded into some new theory. The experimental facts beyond the SM are finite neutrino masses, the baryon asymmetry of the Universe and the existence of Dark Matter (DM). On the theory side, there exists in addition a whole list of arguments pointing in the same direction. Various aspects concerning new physics beyond the Standard Model were therefore studied in the reporting period, applying very different viewpoints and methods to test the ideas.

New Physics at Colliders

The Large Hadron Collider (LHC) provides unprecedented energies to probe the existence of new particles from theories beyond the Standard Model. Moreover, it is the only direct way to probe properties of the Higgs boson. As the Standard Model can't be the final description of nature at fundamental scales, there must be new physics, possibly in reach of the LHC's centre-of-mass energy of currently 13 TeV.

Theories beyond the Standard Model (SM) always predict new particles of all types, fermions, scalars or bosons. In particular left-right symmetric theories, a very elegant and natural extension of the SM, predict three new gauge bosons, require for consistency right-handed neutrinos, and for successful breaking to the SM depend upon new scalar Higgs particles.

Among the three gauge bosons the neutral Z' can be easily looked for, as its decay produces two opposite-sign leptons ("dileptons"). The two charged gauge bosons denoted W_R are more difficult to look for as their decay produces two jets or a charged lepton and a neutrino which escapes undetected. However, in standard left-right symmetric theories the W_R is lighter than the Z' by a fixed factor of about 1.7, and if the mass limit of the W_R is translated into a Z' limit with the help of this factor, it turns out that direct Z' limits are weaker. However, it was noticed that if the gauge couplings of the left- and right-handed interactions are different, or if the left-right symmetry is broken in a different way, the Z' can in fact be much lighter than the W_R. In this case, dilepton data provides the best constraint on left-right symmetric theories [1]. Moreover, the dilepton limit on the Z' can be translated into a limit on the lifetime of neutrinoless double beta decay.

It was also shown how such theories can accommodate various anomalies in the data, such as hints for resonances at about 2 TeV in the di-electron + di-jets channel.

Assessing the sensitivity of future hadron colliders to the scalar sector of left-right symmetric models, it was concluded that the heavy Higgs sector can be effectively probed up to 15 TeV with a 100 TeV proton-proton collider [2].

A different method to probe new physics is provided by the proposed Large Hadron Electron Collider, which would collide electrons with protons. As the electrons can be polarised, it provides an excellent opportunity to test the right-handed nature of the interaction in left-right symmetric theories. It was shown [3], using different potential configura-

tions of the LHeC, that right-handed neutrinos up to masses of 1 TeV and W_R up to 5 TeV are reachable, and that the testable parameter space is complementary to the one of the LHC and of neutrinoless double beta decay. The usually neglected electron misidentification was demonstrated to be an important source of background. Nevertheless, the LHeC is not only a precision machine, but also has the potential to be a discovery machine.

Regarding properties of the Higgs particle, hints of nonstandard decays into muons and taus were interpreted. Moreover, within models containing a very light scalar particle coupled to the Higgs boson, its decay into three of these light scalars was studied. Model-independent conditions which the scalar sector after electroweak symmetry breaking has to satisfy in order for the three-body channel to become relevant exist, and were shown to allow for scenarios in which the rates of scalar three-body Higgs decays are comparable to or even exceed those of the well-studied two-body channel. Such three-body Higgs decays can lead to exciting new collider signatures with six SM fermions in the final state, and it was demonstrated that e. g. six-muon or six-tau final states may be in reach of dedicated searches at the LHC or ILC experiments [4].

Lepton Flavour Physics

In the quest for the high-energy completion of the Standard Model (SM) of particle physics, it is vital not only to look for direct signatures of new physics at colliders. Instead, one should also study the effects which currently inaccessible physics might have on low-energy observables. The persisting absence of new physics at the LHC indicates that new physics may live at much higher energy scales than current experiments can access. Therefore, one could think of such low-energy measurements as being our telescope to get a glimpse of what comes far beyond the SM.

A prime example of such an observable is the decay of one charged lepton into another, lighter charged lepton of a different 'flavour' plus a photon that carries away the difference in energy. Although such decays are strictly forbidden in the SM, they are expected to occur at a tiny rate due to the nonzero mixing of neutral leptons, as manifest in neutrino oscillation experiments. For the SM muons, taking into account this effect only, one expects a branching ratio of roughly 10^{-55}. This negligibly small number is readily enhanced by augmenting the field content of the SM yielding typically sizeable contributions to the branching fraction. As an example, we have studied the implications of lepton flavour violation (LFV) on a model of loop-induced neutrino masses and dark matter. Neutrino masses are generated radiatively by one-loop processes involving new fields, while the dark matter candidate is the lightest neutral particle among them. The conclusion of this analysis is that neither collider searches, nor direct or indirect detection of the dark matter candidate give considerable constraints on the parameter space. Instead, LFV is a promising observable for the verification or falsification of this setup. Future $\mu \to 3e$ and μ-e conversion experiments, in particular, have the potential to probe the entire viable parameter space of this model.

On the other hand, the very same amplitude that enhances the LFV decay described above will contribute to the leptons' magnetic moments. From quantum mechanical considerations, one expects the magnetic moment of an elementary fermion to be enhanced by a factor of g = 2. However, loop corrections to this g-factor, calculable in quantum field theory, shift its actual value away from 2. The measurement of the electron's so-called anomalous magnetic moment ($g_e - 2$) has lead to the most precise measurement in the history of modern physics: the determination of the electromagnetic fine structure constant with a precision better than one part in a billion.

A similar effort is undertaken to measure the muon's anomalous magnetic moment ($g_\mu - 2$). Previous experiments indicate a slight deviation of the measured ($g_\mu - 2$) from the SM prediction with a statistical significance of about 3.3σ. However, it remains unclear whether or not this is due to new physics, or some not yet fully understood hadronic contribution. In the case that this excess prevails in future experiments, and the errors on the hadronic contributions are under control, we may be facing a new era in particle physics. As previously stated, both phenomena – LFV decays and the ($g-2$) – are intimately correlated. While the latter seems to indicate the presence of new physics, the former tightly constrains many theories beyond the SM as recently reviewed in Ref. [5]. In this reference it was shown that, if the upcoming experiments should verify the new physics origin of the anomaly in ($g_\mu - 2$), many popular models also predict a signal for LFV. Conversely, if this

anomaly is resolved otherwise, e. g. by hadronic uncertainties, the high accuracy of the ($g_\mu - 2$) measurements will give important constraints on LFV. In either case, any potential signal must be reconciled with all available constraints and thus, it is of great interest to the high-energy physics community to have these tools ready when a positive signal is observed. In the meantime, more theoretical work is needed, extending existing analyses to other LFV decays, such as $\mu \to 3e$ or muon-electron conversion in nuclei, and furthermore including constraints due to, e. g. dark matter, neutrino physics, and collider searches.

Hierarchy Problem

One of the most severe theoretical problems in particle physics is the so-called hierarchy problem of the Higgs boson mass. It was discussed and studied long before the discovery of the Higgs particle. However, as the LHC has confirmed the existence of the Higgs field the question why its mass is relatively small, in comparison with other scales we expect to exist in nature, becomes more pressing than ever. For a long time Supersymmetry (SUSY) was the most popular attempt to solve the hierarchy problem and other way around the hierarchy problem is the strongest argument for low-energy SUSY. However, as the LHC cuts deeper in the SUSY parameter space without any hints for the existence of this theory, other approaches are needed.

An often used explanation which has been explored is based on the idea that no explicit mass scales exist in nature, but are rather spontaneously generated by dynamic processes. The symmetry forbidding explicit mass scales is called conformal symmetry.

Starting with this assumption, that the theory must not contain any dimensional parameters, different methods have been studied in order to spontaneously generate scales and masses. Two major directions have been pursued. On the one hand the spontaneous mass scale generation can be achieved by strong dynamics, as known from quantum chromodynamics [6]. The electroweak symmetry breaking is triggered here dynamically via the Higgs portal by the condensation of the coloured scalar field around 1 TeV. It can be produced at the LHC. This non-perturbative generation of the electroweak scale can serve as a new starting point for more realistic model building in solving the hierarchy problem.

The other possibility is the mechanism named after Coleman and Weinberg which is weakly coupled at all scales and generates energy scales spontaneously by radiative symmetry breaking and inducing vacuum expectation values of the Higgs and other scalar fields. This framework has been implemented in a set of models which are designed to explain the fact that neutrinos have a small but non-vanishing mass [7]. Within these scale-invariant models neutrino masses and the scale of lepton number violation are detached from each other. This effect roots in the possibility of the existence of small coupling constants which can increase or decrease the scale of lepton number violation without changing the resulting value for the neutrino mass. A more detailed study of a particularly interesting model from a phenomenological point of view, the conformal inverse seesaw, was also performed, see Fig. 1. In addition to neutrino mass generation in this model a dark matter candidate emerges at the keV scale. This type of dark matter is not only produced naturally within the conformal inverse seesaw but also can resolve some of the observational difficulties in the dark matter distributions due to a larger free streaming length than more massive particles, which are normally considered as dark matter candidates.

In order to generate energy scales, the underlying conformal symmetry must be broken and indeed it is violated by quantum effects. This fact on the other hand poses a difficulty, as the quantum breaking of conformal symmetry puts in question its validity as protective symmetry to ensure the absence of explicit scales. A possible explanation was proposed by embedding the theory in the context of gravity. In this way at a high-energy scale the quantum effects of gravity and the scalar field sector can compensate each other and ensure the vanishing of the conformal anomaly.

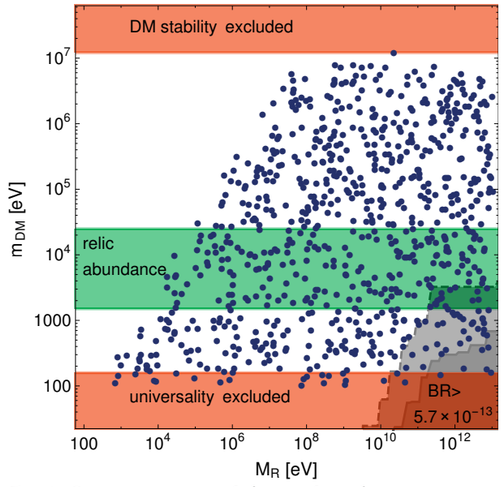

Fig. 1: Parameter space of the conformal inverse seesaw model. Displayed are mass of the dark matter candidate and the induced scale of lepton number violation. Various constraints in terms of sucessful dark matter and laboratory limits are also given.

Inflation and Baryogenesis

Two major indications for the incompleteness of the Standard Model (SM) follow from cosmology: On the one hand, the paradigm of cosmic inflation requires an extended scalar sector, including a so-called inflaton field; on the other hand, the observed baryon asymmetry of the Universe needs to be generated via some sort of mechanism (baryogenesis) that involves new physics beyond the Standard Model. Both aspects of early Universe cosmology, inflation and baryogenesis, are therefore crucial to a better understanding of the completion of the Standard Model at higher energies. In the reporting period, both topics were studied.

Inflation is one of the main pillars of modern cosmology. Not only does it account for the vast size of the observable Universe and its high degree of homogeneity and isotropy on cosmological scales; it also seeds the post-inflationary formation of structure on galactic scales. At present, a consensus about how to correctly embed inflation into particle physics is, however, still pending. In view of this situation, a promising approach appears to be to ask to what other known or hypothetical phenomena in high-energy physics inflation might possibly be connected. Here, an attractive option is to identify the SM Higgs boson itself as the inflaton field. As we studied in more detail, this is a viable possibility, as long as the SM Higgs potential is sufficiently stabilised via new scalar degrees of freedom. Alternatively, inflation might be intimately linked to the spontaneous breaking of supersymmetry (SUSY) – a novel idea that we proposed in [8] and which we dubbed "Polonyi inflation". SUSY offers several particle candidates for dark matter, allows for gauge coupling unification, and sets the stage for a UV completion of the Standard Model within string theory. Since we have not yet seen any superparticles in experiments, SUSY is necessarily broken in Nature. As we have shown, if SUSY is broken at an energy scale close to the scale of grand unification, it may in addition also provide a dynamic explanation for the occurrence of cosmic inflation. This is an intriguing scenario, which yields a new perspective on the interplay between SUSY breaking and inflation within the framework of high-scale SUSY: Inflation is driven by the SUSY-breaking vacuum energy density, while the field responsible for SUSY breaking, the Polonyi field, serves as the inflaton. The mechanism is in accord with the data on the power spectrum of the cosmic microwave background and predicts a large mass for the gravitino, the superpartner of the graviton. While hard to test, if confirmed one day, it would provide strong evidence for "Polonyi inflation", that is, the unification of the dynamics of inflation and spontaneous SUSY breaking.

An elegant way of generating the baryon asymmetry of the Universe is baryogenesis via leptogenesis. In this scenario, one first generates a primordial lepton asymmetry, which is subsequently processed into a baryon asymmetry by sphalerons, non-perturbative effects in the electroweak sector of the Standard Model at high temperatures. In the reporting period, we investigated a particular version of leptogenesis (resonant leptogenesis after sneutrino inflation) and again its possible connection to the spontaneous breaking of SUSY. In addition, we studied the impact of a so-called theta vacuum angle in the electroweak sector on the predictions of various baryogenesis scenarios. While conceptually interesting, it was concluded that a nonzero electroweak vacuum angle leaves the predictions of most baryogenesis scenarios more or less unaffected. On the other hand, our analysis points to the yet unexplored possibility that the electroweak vacuum angle alone could be responsible for the bias between baryons and antibaryons during baryogenesis.

Gravitational Waves

A new window into the Universe was opened in 2016: The LIGO collaboration announced the first direct detection of gravitational waves. It is therefore especially interesting to consider particle physics models and effects which are extremely hard to test in laboratories but which could be probed by gravitational waves.

The thermal history of the Universe still remains a big mystery and many models beyond the Standard Model of particle physics predict enhanced symmetries at high energies. Two prominent examples are high-scale supersymmetry and Peccei-Quinn symmetry. Since we do not observe these symmetries at low-energy scales, they have to be broken. This symmetry breaking can give rise to strong first-order phase transitions which spread out through the Universe via bubble nucleation. Thereby, collisions of bubble-walls create gravitational waves. It was calculated that the LIGO interferometers can test, due to their frequency range, first-order phase transitions at energies of $(10^7\text{-}10^8)$ GeV. This is far beyond any energies which can be produced in laboratories and thus an invaluable test of high-energy physics.

Observations such as the cosmic microwave background show that only ~5% of the energy content of the Universe is baryonic matter. About ~27% of the energy content is a yet unknown form of matter which was named dark matter. One particular theory of dark matter suggests that it is formed by ultra-light bosons with a mass of $(10^{-22}\text{-}10^{0})$ eV which form a Bose-Einstein condensate. If dark matter halos are Bose-Einstein condensates of galactic size, then a gravitational wave passing through the halo will excite phonons which introduce a mass for the graviton in the Bose-Einstein condensate and thus alter the propagation speed of the gravitational wave. We have shown that such a change in propagation could be measurable by future multi-messenger searches which search the sky for correlated gravitational wave, light and neutrino signals [9]. Testing Bose-Einstein condensate dark matter is difficult and thus gravitational waves could be a unique opportunity to clarify the nature of dark matter.

Other Topics

The theoretical particle physics work at MPIK has covered a large variety of topics. And so a number of publications cannot be attributed to any of the subject categories covered so far.

The stability of the proton in the framework of unified theories has been addressed by a series of publications. The first experiments which have set lower limits on the proton lifetime have pushed the scale of all up to now known theories for force unification to a mass scale close to the fundamental scale of gravity, the Planck scale. This makes the hierarchy problem extremely pressing and manifest even if low-scale SUSY was realised in nature. Motivated by this problem theories have been studied, in which baryon number is lifted to a local symmetry and spontaneously broken. However, the breaking is such that the proton cannot decay even though the scale of symmetry breaking can be slightly above the electroweak scale. Within this theoretical embedding interesting phenomena have been studied. On the one hand the possibility has been explored that unification is much lower than expected in traditional unification theories [10]. Furthermore, models with gauged baryon number can lead to an automatically stable dark matter candidate, which can induce gamma-line signatures.

Other studies include phenomenology of supersymmetric theories in which R-Parity is violated, which were shown to produce distinct signals in the IceCube experiment. Furthermore, in a dedicated study the possibility was explored to constrain new physics, formulated in terms of dimension-6 operators suppressed by high-energy scales, with precision measurements of the Higgs boson properties [11]. Those measurements could be performed at a future electron-positron collider and can reach new physics scales of up to 10 TeV.

Manfred Lindner, Sebastian Ohmer, Moritz Platscher, Farinaldo da Silva Queiroz, Juri Smirnov, Kai Schmitz

References:

[1] S. Patra, F.S. Queiroz, W. Rodejohann, Phys. Lett. B 752, 186 (2016)
[2] P.S.B. Dev, R.N. Mohapatra, Y. Zhang, J. High Energy Phys. 1605, 174 (2016)
[3] M. Lindner, F.S. Queiroz, W. Rodejohann, C.E. Yaguna, J. High Energy Phys. 1606, 140 (2016)
[4] A.J. Helmboldt, M. Lindner, arXiv:1609.08127
[5] M. Lindner, M. Platscher, F.S. Queiroz, arXiv:1610.06587
[6] J. Kubo, K.S. Lim, M. Lindner, Phys. Rev. Lett. 113, 091604 (2014)
[7] M. Lindner, S. Schmidt, J. Smirnov, J. High Energy Phys. 1410, 177 (2014)
[8] K. Schmitz, T.T. Yanagida, Phys. Rev. D 94, 074021 (2016)
[9] P.S. Bhupal Dev, M. Lindner, S. Ohmer, arXiv:1609.03939
[10] P. Fileviez Perez, S. Ohmer, Phys. Rev. D 90, 037701 (2014)
[11] S.F. Ge, H.J. He, R.Q. Xiao, J. High Energy Phys. 1610, 007 (2016)